ROMANIA
”Dunărea de Jos” University of Galați
The School for Doctoral Studies in Fundamental and Engineering Sciences

PhD Thesis

- RESUME -

Contributions to the development of a system for monitoring losses on high voltage power lines by surveillance with unmanned aerial vehicle

PhD Student:
Cpt. ing. Cristian VIDAN

Scientific Coordinator:
Prof. univ. dr. habil. ing. Marian GĂICEANU

GALAȚI
2020

Acknowledgments

At the end of my doctoral internship, I feel honored to address words of sincere thanks and feelings of choice to Mr. Prof. Univ. Dr. habil. eng. Marian GĂICEANU, for the support, trust, patience and encouragement, given in the difficult moments that appeared during the elaboration of the doctoral thesis. The suggestions I received and the frequent discussions led to the permanent improvement of the thesis writing.

Thank you to the associate professor, Ph.D. Pericle Gabriel MATEI, for the support and constructive suggestions given in the elaboration of the thesis and during the research activity. I would also like to express my thanks to Mr. Prof. Univ. Dr. eng. Adrian FILIPESCU and Mr. associate professor, Ph.D Ion VONCILĂ for the pertinent observations and meaningful suggestions that I had during the presentation of the papers and that led to a significant improvement of the CDC (Corona Discharge Classification) software designed in this paper.

I extend my warm thanks and sincere appreciation to the dean of the Faculty of Aircraft and Military Vehicles, prof. univ. dr. eng. Mihai MIHĂILĂ-ANDRES for the understanding he showed, as well as to the entire team of the Department of Integrated Aviation and Mechanical Systems from the Military Technical Academy “Ferdinand I” where I carried out most of my research activity . I also want to highlight the excellent collaboration and endless debates on technical topics I had with my colleagues from the Center of Excellence "Self-Propelled Systems and Technologies for Defense and Security" of the Military Technical Academy "Ferdinand I".

I would also like to thank the project coordinator “Advanced system for reducing losses in the transport of utilities of strategic interest, based on IT infrastructure and supervision Autonomous Air Force (INSAV) ”, because it had a decisive influence in choosing the title of the thesis.

On this occasion, I would like to warmly thank Mr. Prof. Univ. Dr. habil. eng. Lucian Teodor GRIGORIE for supporting, guiding and collaborating in various research projects that have been the cornerstone of my teaching and research career.

Thanks to my colleagues, Lt. eng. Răzvan Viorel MIHAI and eng. prog. Mihaela MĂRĂCINE for the excellent collaboration in the elaboration of some scientific papers that, in the end, gave consistency to my research activity in the field of electrical engineering, as well as in the aerospace field.

Last but not least, I would like to thank my family, especially my wife, Anca Elena VIDAN, for her patience, understanding and moral support throughout the preparation of her doctoral thesis.

Bucharest, July 2020, Cpt. eng. Cristian VIDAN

Content

Key words

Overhead High Voltage Power Lines, Monitoring, Unmanned Aerial Systems (UAS), Flight Control, Corona Camera, Image Processing, Machine Learning, Artificial Intelligence Algorithms.

The actuality of the subject

An important feature of the contemporary era is the development of scientific and engineering disciplines, that is an essential feature of the knowledge society that seeks to respond to the increasing complexity of economic and social realities that requires interactive and innovative approaches.

Both globally and in our country, there have been concerns recently about the main negative effects associated with Corona discharge, such as: loss of active power in high and very high voltage networks, aging of liquid or solid insulation and disturbances in telecommunication networks.

I chose this topic because I started from the premise that the market economy, in situations of risk and crisis, cannot function without sustainable electricity, and the stability of a country depends, to a large extent, on this. Knowing the losses caused by the Corona discharge is also very important in terms of the market economy because it directly influences the main costs of electricity transporters.

Regarding the degree of study of the research topic, it can be stated that it has been intensely addressed in recent years in various doctoral theses, scientific articles or research projects. In one of these research projects namely: UAV platforms (unmanned aerial vehicles) with dedicated capabilities and support infrastructure, for applications in national security missions (UAVino) from the Sectoral Operational Program Increasing Economic Competitiveness, Priority Axis 2 - Competitiveness through CDI, PN-III-P2-2.1-SOL-2016-01-0008, I participated as a member of the research team.

The topic of the doctoral thesis is also important by the fact that it introduced the systems of unmanned aircraft with fixed wing in the process of verification and monitoring of power lines. Until now, maintenance on high voltage lines was performed with the helicopter with a human pilot on board, with the UAV with rotating wing, because it had the feature of flight at a fixed point and with land vehicles (terrain vehicles) with different sensors for detecting defects on power lines.

Also, one of the most current fields of research, namely artificial intelligence and machine learning, were approached in order to process in real time the video data stream received from the optical sensor on board the UAV.

For a structured approach, an overview and a well-defined plan, the doctoral thesis was divided into 3 stages that represented the 3 interim research reports. In turn, these reports were divided into 15 specific objectives addressed during the 8 chapters of the doctoral thesis, presented in this summary in subchapter I.2. The objectives of the thesis, and for their fulfillment, during the research, the main objective of this paper was always taken into account.

The main objective of the doctoral thesis is to develop a system for monitoring losses on high voltage power lines by flying, monitoring and detecting Corona discharge using unmanned aircraft systems.

In conclusion, the doctoral topic is very actual, has a continuous interest from electricity transporters, and from a scientific point of view has a huge potential being connected to areas such as image processing, unmanned aircraft systems and artificial intelligence.

I. INTRODUCTION

Strategic energy has important implications for national security, as a country without its own energy resources is vulnerable to armed conflict, and dependence on other energy powerfull country forces it to enter into disadvantageous transactions in order to maintain the security of its citizens. Thus, for a national balance, energy security is ensured by: maintaining a equable balance between national energy demand and production, optimizing primary energy resources according to the structure of consumption and increasing energy efficiency. Both the diversification of sources and supply routes, as well as the limitation of the dependence on imported energy resources, in the future, represent a priority on which Romania wants to act [1]. This can be achieved by reducing losses, especially on high voltage networks. A large part of the losses on overhead power lines is caused by the discharge of Corona, and to annihilate this phenomenon requires two steps: its detection and replacement of used components, specific to OHPL (Over Head Power Lines), which lead to this phenomenon and implicitly to significant losses and which, in the end, it creates many disadvantages both economically and environmentally.

In recent years, the use of drone systems has increased significantly, both in individual and industrial applications, especially in the monitoring of transmission power lines [6] - [8].

Monitoring of high voltage powerlines networks using unmanned flight equipment (UAV, drone) is a major advantage over the conventional methods used. The advantages of using such an unmanned aerial vehicle system for monitoring high voltage lines are:

- High maneuverability;
- Ability to follow a pre-established flight plan;
- Small aircraft dimensions;
- High resolution optical sensor;
- Low flight costs;
- The human operator is outside the risk area;
- Large coverage area;

For static inspections, which do not require a long flight, are used unmanned aerial systems with rotating wing (quadcopter, hexacopter, octacopter, etc.), [20], [21] as well as specialized climbing robots, coupled to the conductor of high voltage lines , which are able to cover the entire length of the conductor and identify any damage or loss [22]. Thus, these robots must remain anchored by the conductor, to cross obstacles along the power line, thus requiring complex robotic mechanisms.

Also, in the field of robots specialized in OHPL inspections, a hybrid robot [24] was developed, capable of landing on the conductors of high voltage lines, then behaving like a climbing robot. When it encounters an obstacle along the conductor, such as an electrical insulator, it is able to detach from the conductor, switch to flight mode, and then land again on the same high voltage line, thus overcoming the obstacle encountered.

Also, the development of new technologies has allowed fixed-wing aircraft to land on high-voltage lines using the electromagnetic field generated by the OHL and an inertial unit of measurement (IMU) to determine the attitude of the UAV in flight. In the paper [26], an experimental system for detecting the electromagnetic field generated by high voltage power

lines is designed from a distance of 4 meters. Thus, with the help of the state estimation block and with a very precise Kalman filtering, it was possible to land on the high voltage lines as well as to charge the batteries by electromagnetic induction [27], [28], in a short time, thus leading to the resumption of flight. and continuing the inspection process.

The difference between flying robots, including fixed-wing UAVs or multi-rotor UAVs, and climbing or hybrid robots, is that flying robots are flexible enough to overcome various obstacles and have a much better sensor perspective. Also, a fixed wing UAV has the advantage of long flight distance, but it is still too fast to obtain detailed information on high voltage lines compared to a rotary wing UAV [29], [30]. Although a UAV with a rotating wing is more maneuverable and has the ability to remain at a fixed point, the short flight time limits its ability to inspect long distances.

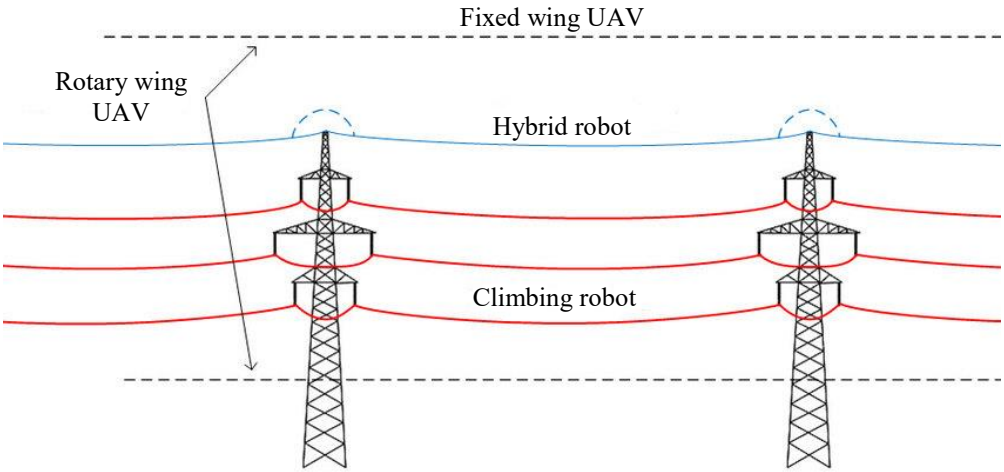

Fig.1.4. Inspection of high voltage lines with different autonomous systems [24]

In fig.1.4. an overview of the different types of autonomous systems capable of carrying out detailed inspections on high-voltage lines is presented.

In the case of Corona discharge, which is a phenomenon whose occurrence is not so frequent and invisible to the human eye, the use of fixed-wing UAVs may be the best solution. Equipping these UAVs with the Corona camera [32] or even the IR camera [33], if the damage to the mains is in an advanced stage, is one of the topics studied in the thesis that led to interesting results.

Corona discharge detection technology using UV spectrum imaging is the basis of maintenance on high voltage overhead lines [34] - [36]. With the help of UV technology, photons with the wavelength specific to the UV signal can be captured, and then they are superimposed with radiation in the visible spectrum to determine the location of the Corona discharge, and the Corona intensity is determined based on the number of captured photons.

In references [43] and [44], the Corona discharge rate at various applied voltages was studied, and based on the analysis of images in the UV spectrum, this discharge rate was determined. Also, in reference [45], several factors that influence the accuracy of Corona detection in UV images were studied, including the number of photons captured, the detection of the distance from the camera to the place where the discharge takes place, the discharge capacity.

In this paper, a Corona discharge detection method is conceived, designed and presented which is based on the processing and analysis of the video data stream received from a Corona camera arranged on board a fixed wing UAV. Also, during this paper are presented the advantages, but especially the disadvantages of the appearance of Corona discharge on high voltage power lines, an autonomous flight scenario with a fixed wing UAV system that is able to fly over high voltage power lines in different relief areas based on a flight route created especially for OHPL. Also, the overflight of high voltage lines with UAV systems with fixed wing, as well as the development of the Corona discharge classification algorithm, part of the CDC (Corona Discharge Classification) software, are some of the novelty elements of this doctoral thesis.

I.1. Thesis motivation

The main motivation for starting doctoral studies in this field is the need for electricity transpoters to reduce losses on high voltage power lines. The early detection of the most dangerous factor leading to power losses, namely the discharge of Corona, is another challenge for many teams of researchers and a huge interest from companies that provide maintenance on overhead power lines. Also, another factor that led to the beginning of this study was the introduction of unmanned aerial vehicle systems with fixed wing in the process of checking and monitoring power lines. Until now, maintenance on high voltage lines was performed with the helicopter with a human pilot on board, with the UAV with rotating wing, because it had the feature of flight at a fixed point and with land vehicles (terrain vehicles) with different sensors for detecting defects on power lines.

Another motivation for starting doctoral studies and approaching this topic is given by the fact that the field of UAV is constantly expanding both in terms of missions that can be performed by air carriers and in terms of constructive solutions. The successes of UAV systems in military operations have influenced the growing interest among the armed forces and civilian companies in their use. The development of nanotechnologies, opto-electronics, as well as the perspective of using intelligent materials can make it possible to carry out increasingly complete UAV projects, capable of performing missions in both civilian and military fields.

Also, artificial intelligence and machine learning are still in their infancy and can provide unexpected results during research. In this paper, I set out to create a Corona discharge classification block based on artificial intelligence algorithms, which is an additional motivation for the successful completion of the doctoral thesis.

I.2. Thesis objectives

For a structured approach, an overview and a well-defined plan, the doctoral thesis was divided into 3 stages that represented the 3 interim research reports. In turn, these reports were divided into specific objectives which, in order to achieve them, during the research, the main objective of this paper was always taken into account.

The main objective of the doctoral thesis is the development of a system for monitoring losses on high voltage power lines by flying over, monitoring and detecting Corona discharge using unmanned aircraft systems.

In order to achieve the main objective of the thesis, I set out to meet the following specific objectives, as follows:

OS1: Documentation on the current state of use of unmanned aerial vehicle (UAS) systems on high voltage power lines to detect Corona discharge.

OS2: Study on high voltage overhead power lines in Romania and other countries, the mode of electricity transmission and documentation on the execution of specific OHPL maintenance procedures.

OS3: Study on voltage losses on overhead power lines caused by Corona discharge, methods for detecting and classifying Corona discharge.

OS4: Calculation of losses caused by Corona discharge by developing a numerical simulation model of a 400 kV high voltage line.

OS5: Analysis of existing unmanned aerial vehicles (UAS) systems capable of performing OHL loss detection missions.

OS6: Study of sensors used in unmanned aerial vehicle systems, communication channels, UAS data types and flight control methods.

OS7: Design of the technical solution of the flight platform and of the sensors arranged on board it.

OS8: Design of the technical solution of the payload on board the UAV and integration with avionics equipment.

OS9: Design of the UAV altitude control system and analysis of the results obtained by numerical simulation.

OS10: Analysis of the flight parameters of the UAV system for a predetermined flight scenario in order to follow the high voltage overhead power lines.

OS11: Design of the system for interpreting the video data received from the Corona sensor located on board the UAV.

OS12: Mathematical demonstration of the functionality of the component blocks of CDC (Corona Discharge Classification) software.

OS13: Design and software development of the Corona discharge classification block using data entrainment algorithms.

OS14: Choosing the classification algorithm with the best performance, after checking the score, accuracy and training / testing times for a data set that has not been processed.

OS15: Analysis and interpretation of the results obtained, ways of using the results and proposals for further development.

The specific objectives presented above are addressed during the 8 chapters of the doctoral thesis, being presented comments, analyzes and the mode of achieving the objectives, at the end of each chapter.

II. CORONA DISCHARGE AND THE ELECTRICAL NETWORK OF ROMANIA

In Romania, the electricity distribution and transmission networks are characterized by an advanced degree of physical wear (about 65%) of low, medium and high voltage power lines, transformer stations and transformer substations. To this is added the moral wear, 30% of the installations being equipped with equipment produced in the '60s. Own technological consumption in distribution networks (including trade losses) as an average annual value is higher than the EU average of 7.3% [1].

The Romanian electric transmission network (RET) is presented in fig. 2.1. and consists of several sections of overhead lines on which electricity flows at different voltages.

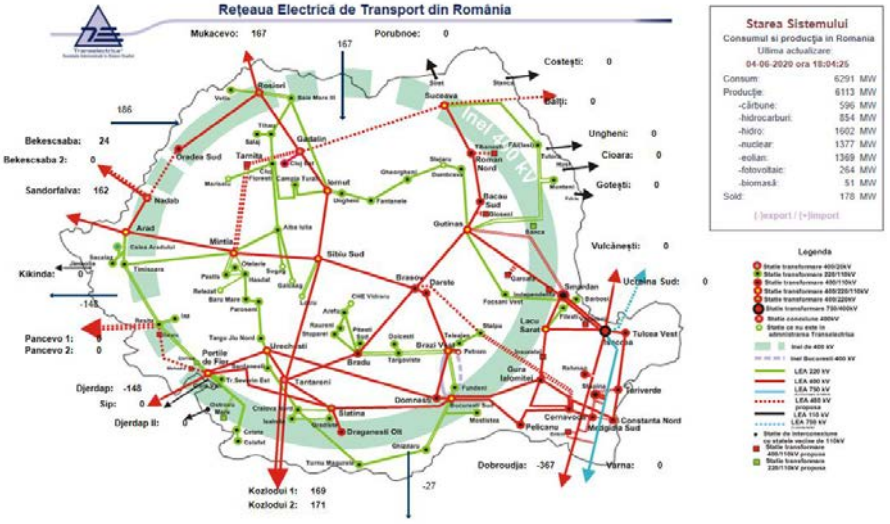

Fig. 2.1. Arrangement of high and very high voltage powerlines in Romania [1]

It is observed that 97% of the length of Romania's electricity transmission line is made up of 220 kV and 400 kV overhead power lines with a total length of 8,731.63 km. Therefore, attention to the losses of active power caused by the discharge of Corona will be directed to these voltages.

II.1. Corona discharge

High-voltage overhead power lines (with a rated voltage greater than or equal to 110kV) carry electricity from power generation sources (power plants) to substations near cities. At these very high voltages, a phenomenon called Corona discharge is formed.

Corona discharge is an autonomous process that occurs around an electrode with a small radius of curvature, in the case of applying a voltage equal to or greater than a minimum value depending on the geometric characteristics of the electrode and the environment in which it occurs [70].

The presence of Corona discharge substantially reduces the reliability of the electricity transmission network, leading to a degradation of its insulation. Even if the Corona discharge is an energy process that occurs rarely, over long periods of time, it can severely degrade the

dielectric materials in the insulation. Thus, the effects of this phenomenon accumulate or may become permanent, and the penetration of the insulators may occur without warning.

At an advanced stage, Corona discharge is accompanied by light phenomena (violet light corona around conductors), acoustic (specific noise characterized by a continuous hum or crack), chemical (ozone and the production of nitric acid that can attack insulating fittings) . Also, due to the exposure of the components of the electrical network to the Corona discharge, mechanical erosions of the surfaces caused by ion bombardment, heating of the insulators and carbon storage leading to the production of electric arcs can occur [76].

A first classification of the Corona discharge can be made according to the form of the applied voltage, namely:

- DC voltage discharge;
- AC voltage Corona discharge;
- discharge Corona of the impulse.

A second classification can be made from a phenomenological point of view. Thus, the Corona discharge can be unipolar or bipolar.

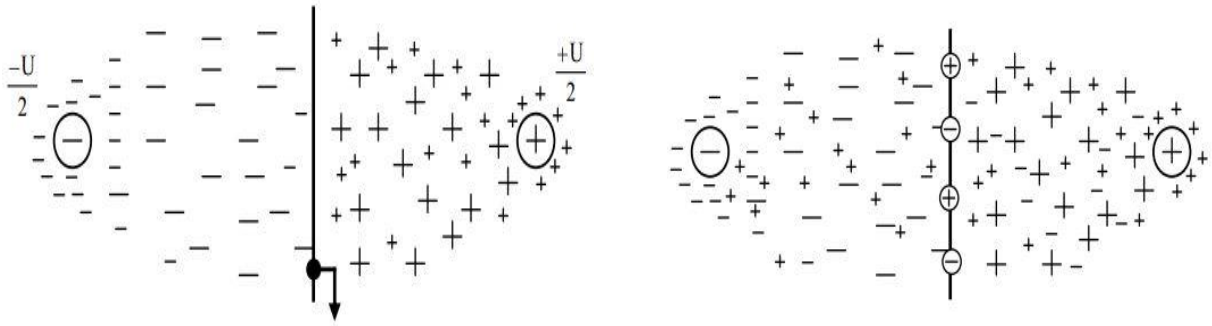

a. Unipolar Corona discharge b. Bipolar Corona discharge

Fig. 2.5. Corona discherge types [70]

Depending on the polarity of the voltage applied to the electrode with a small radius of curvature, there are two types of Corona discharge: negative (when the electrode is energized negatively - cathode) and positive (when the electrode is energized positively - anode). These two types of Corona discharge have common features, but also have specific features.

II.2. Calculation of Corona losses on a 400 kV powerline

Knowing the losses caused by the Corona discharge is very important for the market economy because it directly influences the main costs of electricity transporters.

Next, the basic quantities, characteristic of the occurrence of the Corona discharge, are: the initial intensity (E_i), the critical intensity (E_0) of the electric field, the initial voltage (U_i) and the critical voltage of the occurrence of the Corona discharge (U_0) [97].

Considering the object of the paper which refers to the high voltage lines of 220 kV and 400 kV, the following will focus on the structure consisting of two parallel conductors that have a large distance between them (450 - 550 cm). Thus, for distances between conductors greater than 5 m, a decrease in the intensity of the Corona discharge electric field was found by

about 2% [70]. The explanation lies in the fact that at long distances between conductors the discharge of the Corona is no longer bipolar, but unipolar.

Thus, following the latest experimental results performed on a conductor-ground structure with a large distance between the conductors, the initial intensity (E_i) of the Corona discharge electric field is as follows [70]:

$$E_i = 30,3\delta(1+0,298/\sqrt{r_0\delta})[kV/cm] \quad (2.5.1)$$

Where: δ - air density

r_0 - conductor radius

Whereas, for conductors having $r_0 \geq 1$ cm, the following calculation relation of the initial intensity of the Corona discharge electric field is recommended [70]:

$$E_i = 24\delta(1+0,62/\delta^{0,3}r_0^{0,38})[kV/cm] \quad (2.5.2)$$

The intensity of the Corona discharge electric field is dependent on the density of the air. For standard temperature, t = 20^0C and standard atmospheric pressure (760 mmHg) the value of the electric field is about 30 kV / cm, and for any other temperature and any other atmospheric pressure the intensity of the Corona discharge electric field is multiplied by the correction factor of air density, which is determined by the following formula:

$$\delta = \frac{p}{273+t}\cdot\frac{273+20}{760} = 0.386\frac{p}{273+t} \quad (2.5.3)$$

The loss of active power on the network is a function of the air density correction factor and the higher its value, the smaller the losses. At low atmospheric pressure and high temperatures, the value of the disturbing critical voltage is low and the Corona discharge and implicitly the losses are dominant.

Thus, the initial electric field strength corresponds to the initial Corona discharge voltage for a conductor located at ground level and determined by the following equation [70]:

$$U_i = m_1 m_2 E_i r_0 \ln\frac{2h}{r_0} \quad (2.5.4)$$

Where: m_1 - coefficient that takes into account the condition of the conductor ($m_1 = 0.8-0.87$)

m_2 - coefficient that takes into account atmospheric conditions ($m_2 = 0.8-1$)

For twisted conductors used on 400 kV high voltage lines, m_1 = 0.8 shows a state of advanced conductor damage, and m_1 = 0.87 shows that the conductor surface shows no signs of advanced damage [96].

The coefficient that takes into account the meteorological conditions, is interpreted as follows: m_2 =0.8 - represents unfavorable weather conditions (frost, rain), and for m_2 =1 - weather conditions are the standard ones (t = 200C, p = 760mmHG) [96].

The first to propose a formula for calculating Corona's losses was the American engineer F.W. Peek. It is necessary to mention that the methods of experimental investigation were at that simple time, but the relations determined by Peek are still valid today.

Peek's equations are valid for Corona losses that have reached the stage where the phenomenon can be observed visually, ie. a relatively advanced stage. Thus, the

equation for calculating the Corona losses given by Peek is as follows [96]:

$$P_c = \frac{241}{\delta}(f+25)\sqrt{\frac{r_0}{d}}(U_f - U_i)^2 \cdot 10^{-5}[kV/km/faza] \quad (2.5.5)$$

Where: P_c - corona losses in kV/km/phase

f - AC frequency

U_f - voltage on phase

U_i - Corona discharge initial voltage

δ - air density

r_0 - conductor radius

d - distance between conductors

Currently, there are modern construction techniques for high and very high voltage transmission lines that have a loss by discharging Corona for ideal weather conditions ($m_2 = 1$) from 0.1 to 0.2 kW / km / phase [96]. In this very short range of Corona losses, Peek's relationships can lead to inaccurate results. Therefore, in order to avoid these inaccuracies, when the ratio between phase voltage and initial voltage, $(\frac{U_f}{U_i}) \le 2$, Peterson's formula [98] - [100] is used to determine the losses caused by the Corona discharge:

$$P_c = 2.1fF\left(\frac{U_i}{\log_{10}(d/r)}\right)\cdot 10^{-5}[kW/km/faza] \quad (2.5.6)$$

Where F, it is known as the Corona loss function or the Corona experimental factor, which can be determined according to the $\frac{U_f}{U_i}$ ration that is presented in table 3.

Table 3: Corona experimental factor values according to the $\frac{U_f}{U_i}$ ratio

U_f/U_i	F	U_f/U_i	F	U_f/U_i	F	U_f/U_i	F
1.00	0.037	1.26	0.120	1.52	1.10	1.78	4.72
1.02	0.039	1.28	0.136	1.54	1.33	1.80	4.95
1.04	0.042	1.30	0.154	1.56	1.59	1.82	5.17
1.06	0.045	1.32	0.176	1.58	1.88	1.84	5.39
1.08	0.048	1.34	0.200	1.60	2.20	1.86	5.60
1.10	0.052	1.36	0.228	1.62	2.52	1.88	5.81
1.12	0.057	1.38	0.260	1.64	2.83	1.90	6.01
1.14	0.063	1.40	0.300	1.66	3.13	1.92	6.21
1.16	0.069	1.42	0.38	1.68	3.42	1.94	6.41
1.18	0.075	1.44	0.48	1.70	3.70	1.96	6.61
1.20	0.082	1.46	0.60	1.72	3.97	1.98	6.81
1.22	0.092	1.48	0.74	1.74	4.23	2.00	7.00
1.24	0.105	1.50	0.90	1.76	4.48		

For the calculation of Corona losses, a simulation was performed using the Matlab - Simulink program, which is based on the analytical formulas for calculating Corona losses,

namely, Peek's formula and Peterson's formula. Thus, in fig. 2.9. the scheme for estimating Corona losses is presented, based on the characteristic parameters of the power line and the atmospheric parameters of the environment in which the Corona discharge takes place and which are presented in the following table:

Table 4: Characteristic parameters of a 400 kV powerline and atmospheric parameters in witch the Corona discharge occurs

Parameter name	Parameter symbol	Preset value
Powerline voltage	U_l	400 kV
Distance between conductors	d	550 cm
Conductor radius	r_0	1.2 cm
Height above ground	h	15 m
Frequency	f	50 Hz
Coefficient that takes into account the condition of the conductor	m_1	0.87
coefficient that takes into account the meteorological conditions	m_2	1
Atmospheric pressure	p	760 mmHg
Temperature	t	20°C

The Corona loss calculation model, shown in fig. 2.9, is able to automatically and autonomously select between the analytical method of calculating Corona losses represented by Peek's formula and the analytical method of calculation represented by Peterson's formula. Thus, this selection of the analytical calculation method is made according to the Uf/Ui ratio and implicitly to the experimental factor Corona, F , being able to be made with the help of the *If* block from Simulink, after previously calculated: phase voltage (U_f) and the initial voltage (U_i).

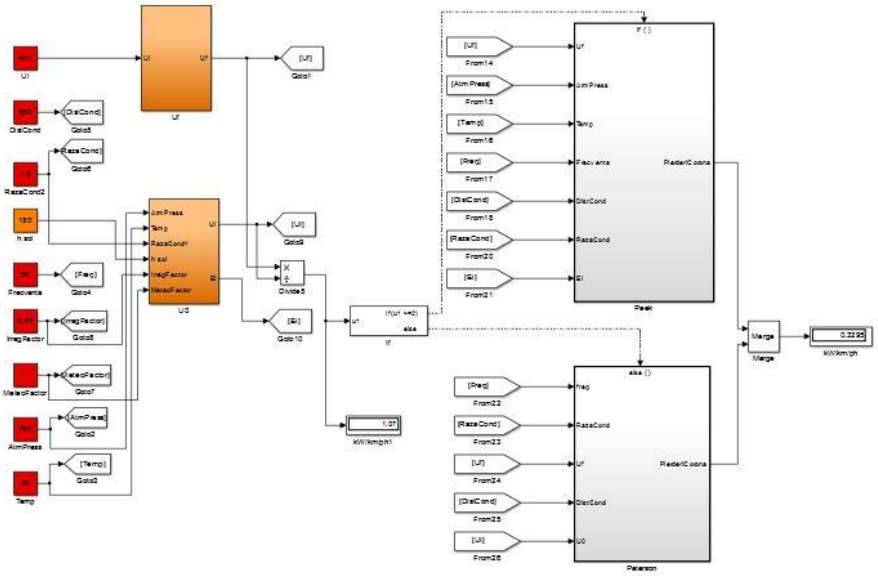

Fig. 2.9. Simulation model of losses caused by Corona discharge

Therefore, by varying the different parameters, both those charcterictics of the 400 kV high voltage power line and the environmental factors, the lossed caused by the Corona discharge can be expressed graphically.

II.2.1. Numerical results obtained

Figure 2.12 shows the graphs of the variation of Corona losses according to the weather factor (2.12.a), the radius of the conductor (2.12.b), and respectively the height from the ground (2.12.c). It should be specified that on the Oy axis the Corona losses in kW / km / phase are represented, and on the Ox axis the values of the analyzed parameters are represented.

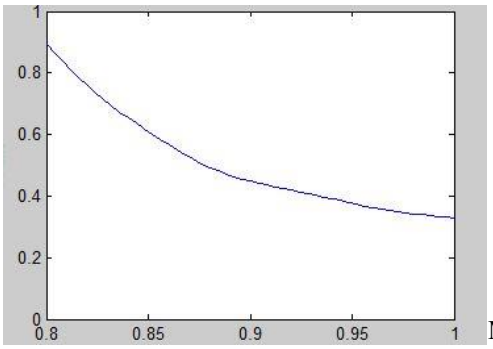

a) Variation of losses depending on the weather factor in MWh

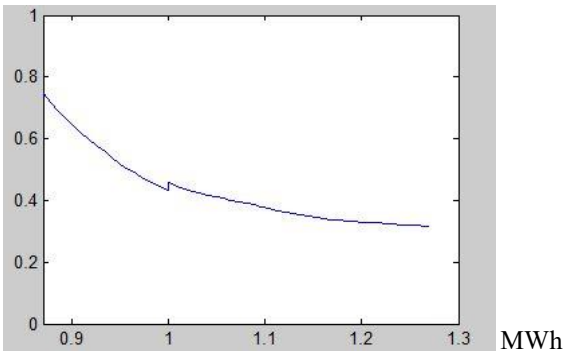

b) Variation of losses depending on the conductor radius in MWh

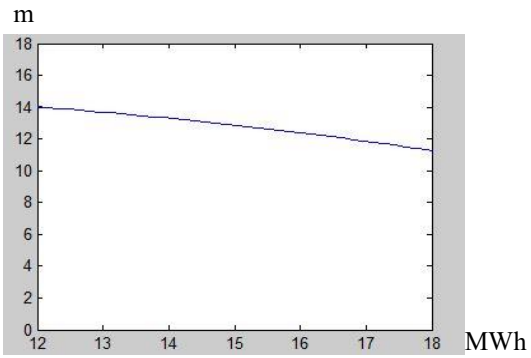

c) Variation of losses depending on the height from the ground

Fig. 2.12 Variations in the losses caused by the Corona discharge depending on various parameters

Thus, it can be seen in graph (2.12.a) that when the weather conditions are favorable, the losses caused by the Corona discharge decrease slightly. The same happens with the radius of the conductor used to transport electricity, the smaller it is, the lower the energy losses. It can also be seen in the graph (2.12.c) that the losses of active power caused by the Corona discharge decrease even more, depending on the height of the conductor relative to the ground, according to the graph (2.12.c).

Following the calculations performed with the numerical simulation model of Corona losses performed in the Matlab-Simulink simulation software, the results are very good, comparable to those performed experimentally on different sections of the overhead power lines in Romania.

III. UNMANNED AERIAL SYSTEMS (UAS)

Unmanned Aerial Vehicle (UAV) is an aircraft that lacks a human pilot, being guided either by a computerized autopilot on board or in another piloted aircraft, or by remote control with a command and control station lying on the ground. A simpler description of this type of air system is that a UAV is, in fact, an aircraft in which flight crew has been removed and replaced with a computer system and a radio link.

Thus, the terminology UAS refers to an entire system of unmanned aircraft that can be composed of ground control stations, the aircraft itself, the communications link, ground support equipment and launch / recovery systems, while the term of UAV refers strictly to the aircraft. Thus, it can be stated that the term UAV is an integral part of a UAS [102] as exemplified in Figure 3.1.

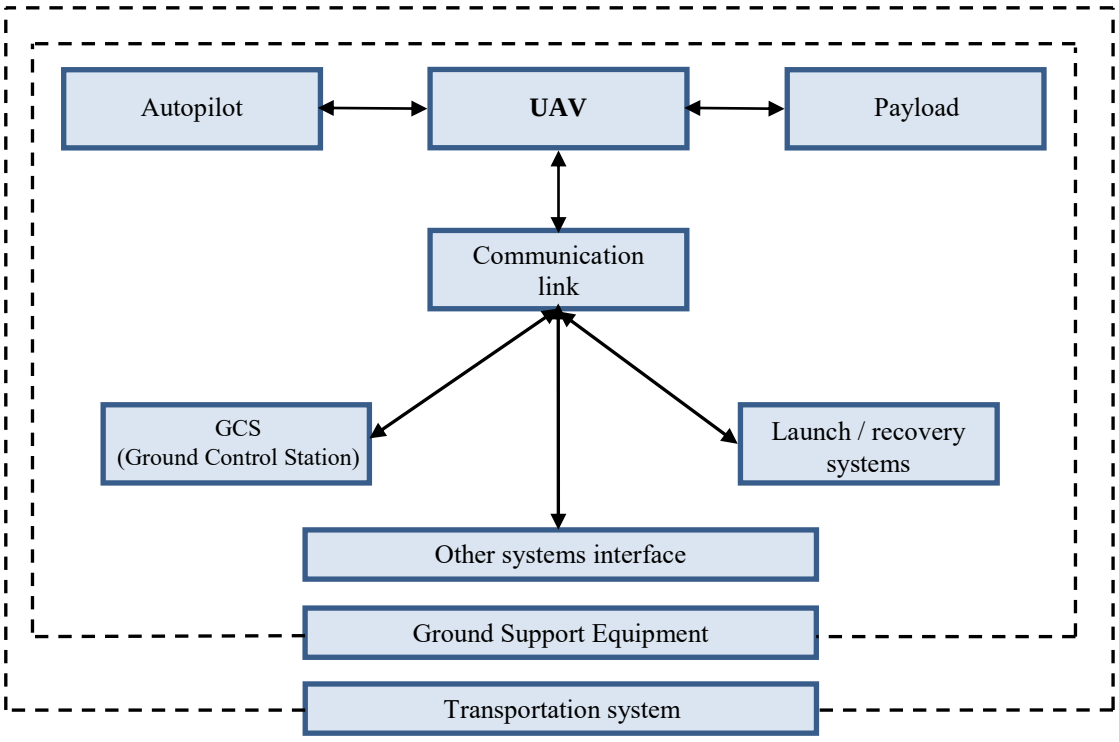

Fig. 3.1. Arhitecture of a UAS

In conclusion, each subsystem in the composition of a UAS is important, and the lack or improper use can lead to accidents both on the maintenance staff and on the system itself.

III.1. Design of the UAV system for flight on the OHPL

When designing the UAV system that will be used to fly over the high voltage lines, the following aspects were taken into account: Romania's relief and the arrangement of the sections of the high voltage lines, the data connection between UAV and GCS, the type of UAV used depending on the specific mission, its flight performance, the design of a flight path specific to the flight on the OHPL and favorable to the detection of Corona discharge. Also, the climate and the environment in which the UAV flies, as well as the level of electromagnetic

field interference around the OHPL conductors are very important aspects in the design of an unmanned aircraft system dedicated to detecting Corona discharge.

For the monitoring, tracking and analysis of high voltage power lines using a UAV system, it is recommended to choose an unmanned aerial vehicle system that best fulfills the tasks and missions received. In conclusion, the variant proposed by this paper for an efficient monitoring of the national high voltage network is a fixed wing UAV. This conclusion was reached by choosing a UAV that does not require a launch and recovery system, so it can be used in any relief area.

III.1.1. Comparative analysis of two sections of OHPL

Before the design itself of the UAV system, it is necessary to carry out a study of the electricity network of Romania, of the relief on which it is placed, as well as the climatic conditions that appear in the regions where the UAV is supposed to fly. In order to demonstrate the need to detect power losses on high voltage networks with the help of a UAV, a comparative analysis of two sections of the high voltage power network (400 kV) that have been established in terms of being located in different relief areas is required. These sections are:

1. Brașov - Bradu;
2. Smârdan - Lacu Sărat - Însurăței – Gura Ialomiței.

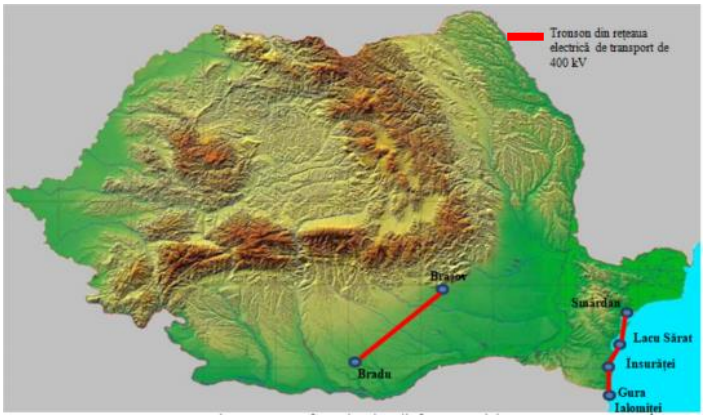

Fig. 3.8. Map of the relief forms of Romania with the sections chosen for the study

The analysis of these sections is performed in terms of their length, as shown in fig. 3.9, as well as from the point of view of the average altitude of the relief of the areas where they pass (fig. 3.10).

Fig. 3.9. The length of the sections of the analysed high voltage lines

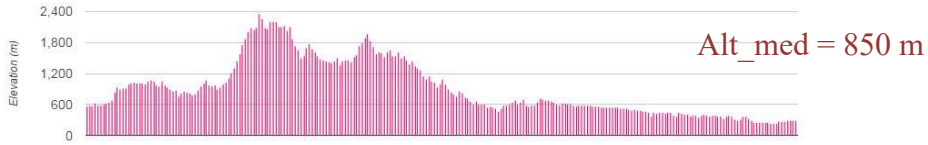

a) The average altitude on the section Brașov - Bradu

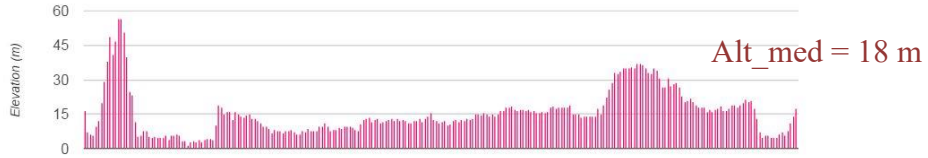

b) The average altitude on the section Smârdan – Lacu Sărat – Însurăței – Gura Ialomiței

Fig, 3.10. The average altitude of the sections subjected to the study

In conclusion, before designing the UAV system that will fly on high voltage airlines, it was necessary to conduct a comparative study between different sections of the OHPL, in order to establish the flight conditions, the communication link between the UAV and GCS and to achieve a critical analysis of the relief forms of Romania, specific for each flight mission.

III.1.2. Design of the flight route of the UAV system

Mission planning and the completion of a flight route is necessary before each take-off and provides the route to be followed by the UAV, consisting of points of interest, hereinafter referred to as waypoints. They are characterized by spatial coordinates (latitude, longitude, altitude), heading information and predefined commands (takeoff, orbit, landing, return to launch, etc.).

The design of a flight route that is, first of all, safe and secondly useful in detecting Corona discharge, has become one of the important aspects of this doctoral thesis. The following factors must be taken into account when designing the flight path:

- ❖ the altitude at which UAV flies;
- ❖ forms of relief;
- ❖ obstacles encountered on the flight path.

Taking into account the factors listed above, a flight route has been created to be loaded into the autopilot memory. This route represents a portion of the 400 kV high voltage line Brașov - Gutinaș and is located at the exit of Podu Oltului vilage, at the border between Brașov County and Covasna County, as shown in Figure 3.11:

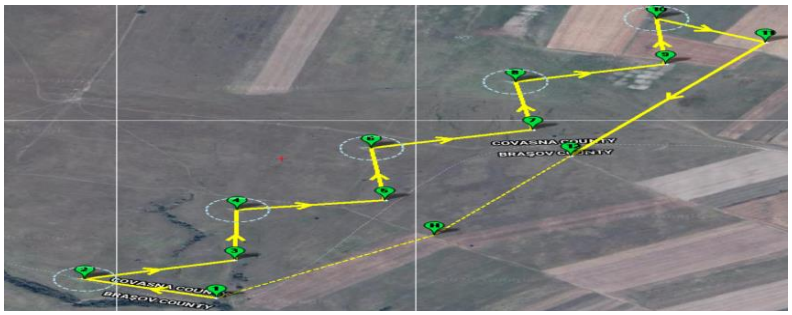

Fig. 3.11. Design of the flight route on the OHPL

In fig. 3.12, the same flight path is shown as in fig. 3.11., But the image is enlarged so that a portion of the flight path can be seen, highlighting the high-voltage pole at the coordinates of which flight points (waypoints) have been configured.

Fig. 3.12. Part of the flight route (enlarge image)

It should be specified that in order to perform flights for the purpose of aerial photography or to fly over critical infrastructure elements, such as high voltage lines, it is necessary to issue a flight approval certificate to be received from ORNISS (Office of the National Registry of State Secret Information).

III.1.3. Design of the unmanned aerial vehicle system (UAS)

This subchapter presents the design of the technical solution and the in-flight testing of an experimental fixed-wing UAV, powered by an electric motor. It should be noted that in the case of a fixed wing UAV, the correlation between aerodynamic performance and stability is not easy to achieve. The design process begins with defining performance requirements, including minimum engagement speed, maximum flight speed, cruising altitude, maximum flight cap, and speed. Thus, the wing area, mass and propulsion of the UAV are determined on the basis of the requirements of flight autonomy and payload. Also, the requirements related to propulsion, determine the size of the engine, and the design of the aerodynamics and stability of the UAV are obtained based on a chosen aerodynamic profile.

Taking into account the type of mission performed, the technical-tactical characteristics of the designed UAV system are presented in Table 8:

Table 8: Technical-tactical characteristics of the UAV system

No. Crt.	Technical-tactical characteristic name	Characteristic value	Remarks
1.	Minimum stall speed	10 m/s	It is the minimum speed at which the UAV can no longer sustain itself in flight
2.	Minimum flight speed	12 m/s	-
3.	Cruise speed	14 m/s	It is used when the UAV moves between high voltage poles
4.	Cruise altitude	100 m	The safety altitude at which the UAV can avoid obstacles in the field
5.	Payload weight	1 kg	Camera weight + gimbal weight = payload weight
6.	Propulsion	electric	-
7.	Minimum flight tine	2 h	The flight time is sufficient to fly over an OHPL route so that the UAV remains in the Line of Sight (LOS)
8.	Minimum radius of orbit	15 m	The radius of the orbit above the poles

III.1.3.1. UAV-ul

The aerial vector (UAV) has the most important role when performing flights over high voltage lines. When choosing the UAV system, the technical-tactical characteristics from table 8 and physical characteristics such as a wing with a large load-bearing surface, sufficient space for the location of the payload and the embarkable electronic systems were taken into account. The zeroing of the control surfaces and the correct arrangement of the weight on board are the basic parameters that must be taken into account when preparing the flight of a UAV. Given the characteristics presented above, the UAV system chosen to carry the optical sensor for the purpose of inspections on high voltage lines is called Sky Walker.

Fig. 3.13. Sky Walker UAV

Following a study compared to other UAV systems in the same class, the Sky Walker UAV best met the requirements expressed in Table 8, becoming the best choice for missions to fly over high-voltage power lines in order to detect Corona discharge.

III.2. Design and numerical simulation of the UAV altitude control system for OHPL flight

For the successful completion of flights on high voltage overhead power lines it is essential that the UAV maintains its predetermined altitude, regardless of changes in the other state variables of the mathematical model.

Controlling the positions of the center of mass in the Earth-related coordinate system (pn, pe, pd) and the attitude angles of the UAV is one of the basic purposes in the construction of a control system.

III.2.1. Customization of the mathematical model of the Sky Walker UAV

In order to simplify the system of equations, the following approximations are made for which the motion of the UAV is based on the hypothesis of the motion in vertical plane, for which:

- the sliding angle is zero, $\beta = 0$
- the angular velocity on the plane of symmetry is zero, $p = 0$
- the lateral force is zero, $f_y = 0$.

In the design of the altitude control system, the longitudinal channel was mathematically described, and as a control structure the cascade control method is used, with different types of classical controllers.

The system of equations from which the design of the UAV altitude control system, on the longitudinal channel, starts is as follows [143]:

$$\begin{cases} \dot{v} = \dfrac{T\cos\alpha}{m} - \dfrac{\rho v^2 S C_x}{2m} - g\sin\theta \\ \dot{\theta} = \dfrac{T\sin\alpha}{mv} + \dfrac{\rho v S C_z}{2m} - \dfrac{g\cos\theta}{v} \\ \dot{q} = -\dfrac{\rho v^2 b S C_{m_\alpha}\alpha}{2J_y} - \dfrac{\rho v b^2 S C_{m_q} q}{2J_y} + \dfrac{\rho v^2 b S C_{m_\delta}\delta_p}{2J_y} \\ \dot{h} = v\sin\theta \\ \dot{\phi} = q \\ \theta = \phi - \alpha \end{cases} \tag{3.6.43}$$

The equations of the mathematical model of the longitudinal channel (3.6.43) underlie the modeling of the Sky Walker aircraft in Matlab. Thus, using the initial data (3.6.44) and the equations (3.6.43), the coefficients of the control structure are determined.

The initial starting date is as follows:

$$\begin{aligned} v_0 &= 10m/s \\ h_0 &= 50m \\ S &= 0.4m^2 \\ b &= 1.68m \\ m &= 4.5kg \\ L &= 1.49m \end{aligned} \tag{3.6.44}$$

The initial data (3.6.44) are specific to the Sky Walker UAV modeled in the Solidworks software according to the physical dimensions and presented in fig. 3.22.

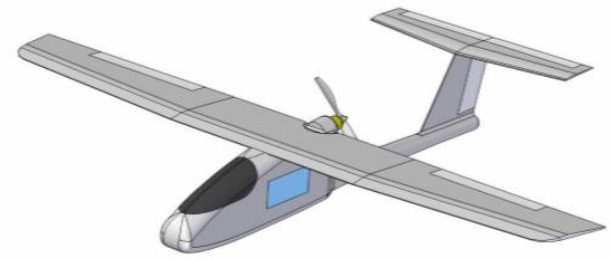

Fig. 3.22. Modelarea UAV-ului Sky Walker în software-ul Solidworks

Solidworks modeling was required to determine the values of the stability derivatives of the UAV. Thus, after modeling in Solidworks, the fuselage, wings, vertical tail and horizontal tail were divided into 20 sections, because the coordinates of these sections were used to

generate a file, being subsequently processed in the DatCom software (Data Compendium), made by NASA and used, freely, by aviation engineers.

Fig. 3.23. Determination of UAV stability derivatives using DatCom software

Always, during the calculation of the aerodynamic coefficients of the UAV, it was taken into account that the main mission of this UAV is to monitor and detect Corona discharge from high voltage lines, which requires a very good equipment in terms of on-board equipment. , due to the danger to which the UAV is exposed, flying quite close to these lines and in a very strong electromagnetic field.

III.2.2. Longitudinal channel modeling in Matlab / Simulink

The Matlab modelling of the Sky Walker UAV starts from the 6 equations of the mathematical model described by the system (3.6.43), to which is added an air density calculation function and several signal display blocks.

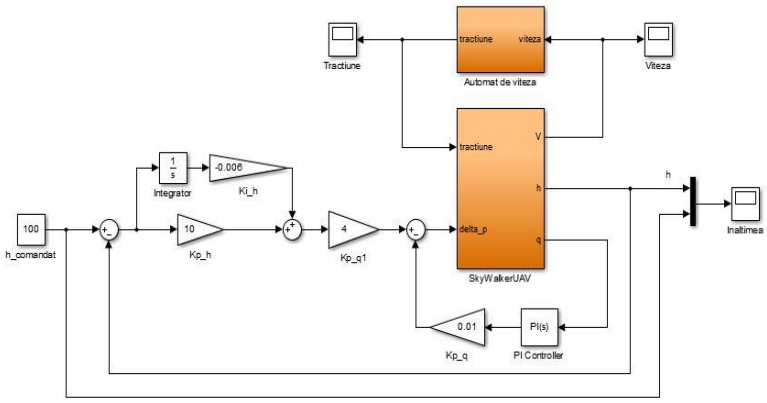

Fig. 3.24. Altitude control system in Matlab - Simulink

In fig. 3.24. the ordered altitude can be observed, h_commanded = 100m. Assuming that the UAV is in flight at a predetermined altitude, h0 = 50m, then the altitude control system starts from the initial altitude value, 50m and will stabilize at a height of 100m.

In the block from Simulink, „SkyWalkerUAV“, are introduced the equations (3.6.43) representing the mathematical model on the longitudinal channel of the SkyWalker UAV, presented in fig. 3.25. Also, to maintain the commanded altitude are used 2 negative feedback loops represented by 2 PI controllers and 2 amplification components represented by the proportionality constants kp_q = 0.01, kp_q1 = 4.

Also, for the control of the altitude, an automatic speed device is used that knowing the initial speed, or the speed of reference and the controlled speed, uses as output value of the automated speed device, represented by the throttle to stabilize the real altitude of the UAV with the controlled one.

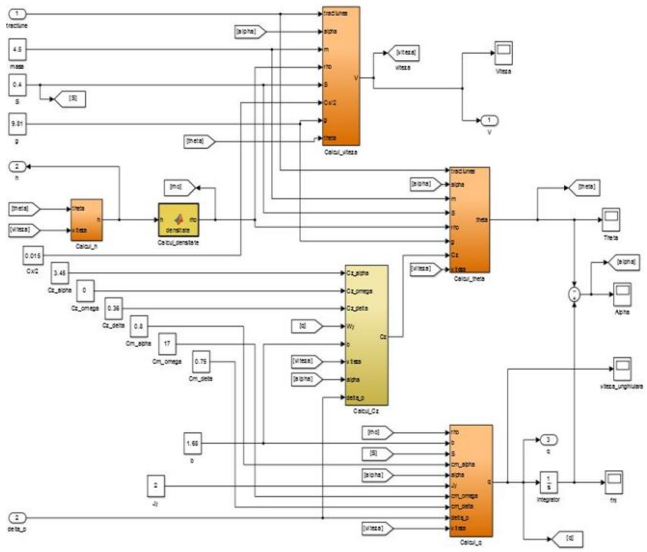

Fig. 3.25. Sky Walker UAV dynamics on the longitudinal channel

III.2.3. Design of automatic speed device

In order to use the flight speed constraint control structures, it was necessary to implement a speed automation that kept the speed constant. Basically, the automatic maintains the constant speed with the help of the throttle control.

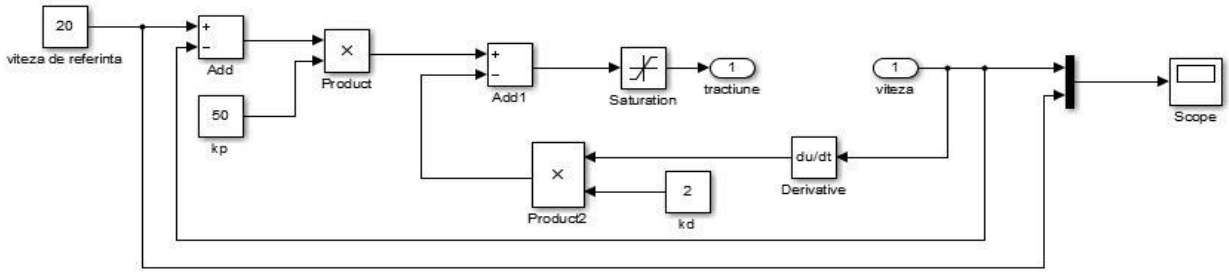

Fig. 3.31. Block diagram of automatic speed device

From the block diagram shown in fig. 3.31, it is observed that the throttle control is performed with the help of a PD type controller, with two feedback loops: one for the speed derivative and one for the speed. The coefficient of the derivative component is denoted by kd, and the coefficient of the proportional component is denoted by kp. The values of the coefficients kd = 2 and kp = 50 were determined by multiple tests, following the evolution of the system.The behavior of the PD type control structure can be analyzed by using a „Scope" type block:

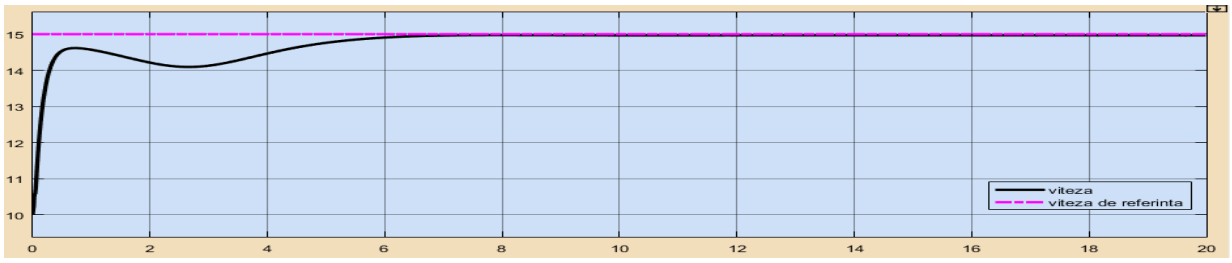

Fig. 3.32. Maintaining constant commanded speed at 15 m/s

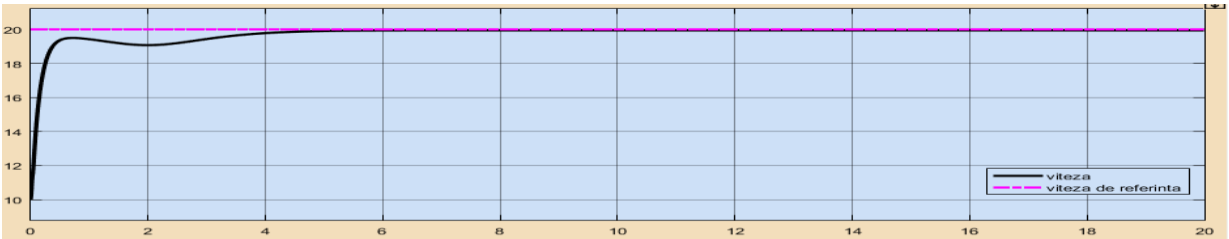

Fig. 3.33. Maintaining constant commanded speed at 20 m/s

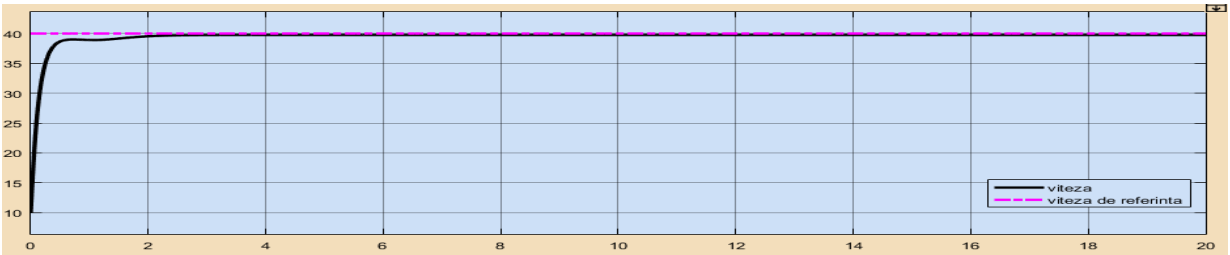

Fig. 3.34. Maintaining constant commanded speed at 40 m/s

Following the analysis of the 3 graphs that indicate the stabilization of the commanded flight speed at 15 m / s, 20 m / s, respectively 40 m / s, considering that, at the time of command, the UAV has a constant flight speed of 10 m / s, it can be concluded that the greater the difference between the commanded speed and the reference speed, the more stable the system. This can be argued by the fact that as soon as the UAV engine increases the speed to reach the controlled speed, the closer it is to the reference speed, the harder it is for the UAV to stabilize at the new speed.

In the graph in fig. 3.35, it is observed, from the throttle diagram, that it has a sudden increase when it is operated, to reach the commanded altitude, then it stabilizes at a value T = 3N, which is sufficient to keep the Skywalker UAV in the air.

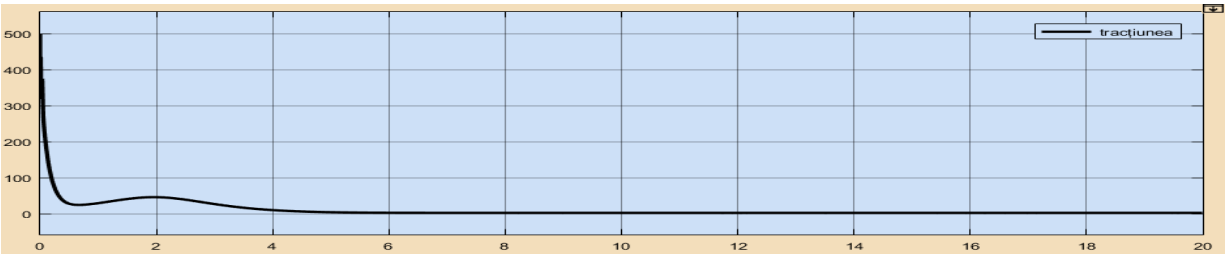

Fig. 3.35. The evolution of the throttle to the command on altitude in N (Newton)

Using the cascade control method, the mathematical model of the longitudinal channel of the Skywalker UAV was stabilized by using 2 PI type controllers (fig. 3.28) and 2 proportional components kp_q = 0.01, kp_q1 = 4.

The PI controller components arranged on the internal negative feedback loop were determined using the Matlab „PID-Tuning“ function, and have the following values: Kp = 177.8 and Ki = 70292.3.

The components of the PI controller, arranged on the control channel, were determined by successive tests, depending on the behavior of the system. They have the following values: Kp_h = 10 and Ki_h = -0.006.

III.2.4. Numerical results obtained

Following the determination of the components of the control structure used, the results obtained are presented in the following graphs:

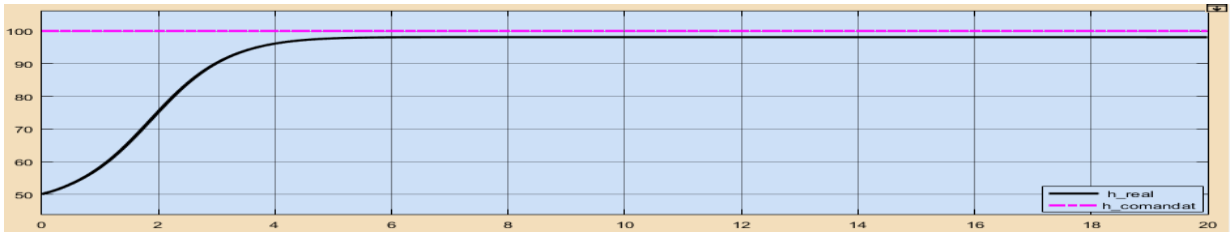

Fig. 3.36. Flight altitude stabilization (in meters)

In figure 3.46, it is observed how the altitude graph starts from the initial altitude h_0 = 50m and stabilizes close to the commanded altitude h_commanded = 100m after a time t = 5s. It is also observed that there is a stationary error in the stabilization band, which has a value of 1.98%, which means that out of 100 m, the altitude at which the UAV has to fly, it reaches the flight altitude of about 98.2 m.

It should be noted that this error can be eliminated by fusioning the data from the barometer with the data from the GPS / RTK system arranged on the Sky Walker UAV.

The evolution of the pitch angle θ, incidence angle α and roll angle φ can be analyzed in the following graphs:

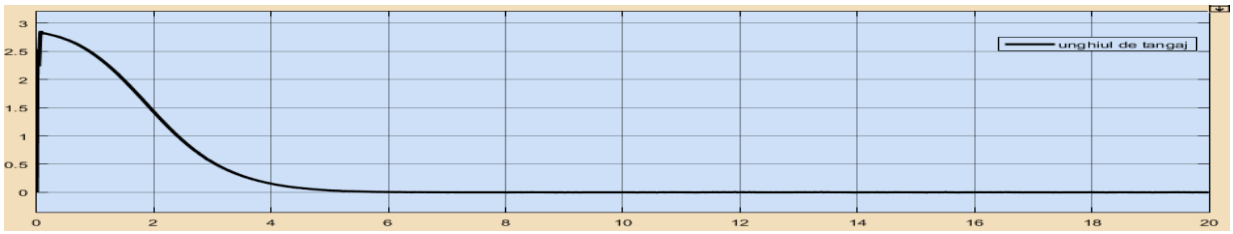

Fig. 3.37. Evolution of pitch angle (in degrees)

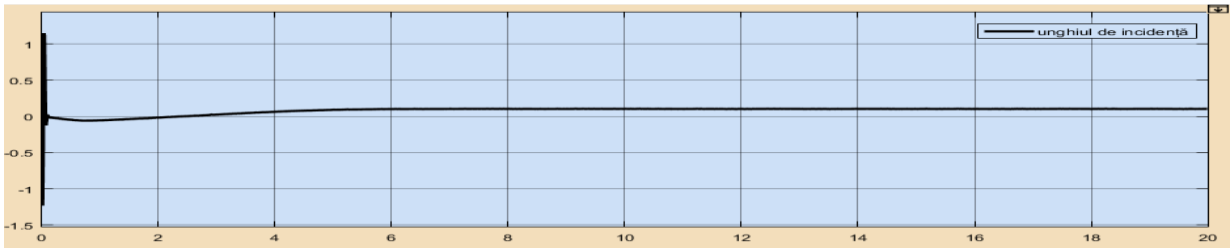

Fig. 3.38. Evolution of incidence angle (in degrees)

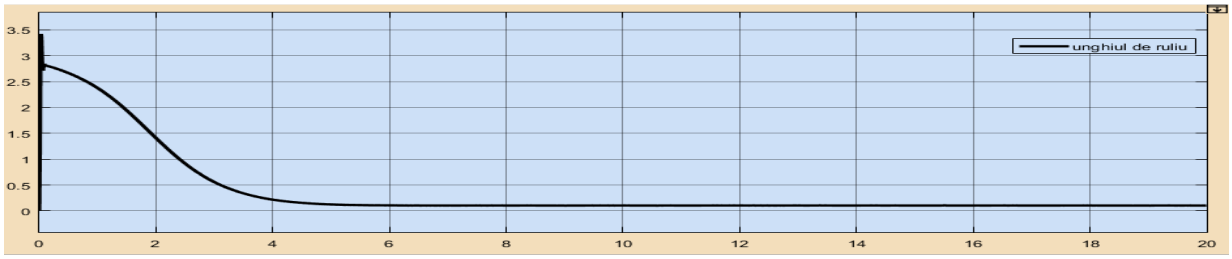

Fig. 3.39. Evolution of roll angle (in degrees)

In conclusion, the design of the altitude control system by stabilizing the UAV on the longitudinal channel, was successfully completed, the commanded altitude being reached in a very short time by the designed UAV.

IV. FLIGHT DATA ANALYSIS OF THE UAV MONITORING SYSTEM

The missions fulfilled by the Sky Walker unmanned aerial vehicle system must be materialized by recording flight data which will then be processed and analyzed in order to extract, the characteristics of interest, from the sensors placed on board the UAV, contributing decisively to flight safety.

Following the construction, in the previous chapter, of a flight path on a 400 kV high voltage line, in this chapter the flight path was loaded in the autopilot memory, together with the components of the control structures determined during the design of the control system. altitude, and the UAV performed several flights on the OHPL, both for calibration and testing, and for the effective detection of Corona discharge. The flight parameters following one of these flights are analyzed in this chapter.

IV.1. Analysis of the flight data of the designed UAV

In order to test the flight capabilities of the UAV over the high voltage lines, several verification flights were performed, on a OHPL section, consisting of 5 poles, of the overhead power line Brașov - Gutinaș, at the border of Brașov and Covasna counties. Following the flights, the data of one of them were downloaded and analyzed leading to very good results which are presented in this chapter.

Thus, following the flight, the specific data were analyzed and small variations in altitude (approximately 5 m) induced by the wind direction were found, the cruising speed remained relatively constant and stabilized at approximately 16 m / s (57 km / h), which makes the system suitable for high voltage line drift, as the cruising speed needs to be kept to a minimum so as to facilitate the capture of Corona images at the best possible quality.

In fig. 4.10, depending on the color (pink, red and yellow), the preset flight modes and loaded in the autopilot memory with the flight path are observed. Thus, the UAV was taken off in AUTO mode - the color pink, specific to the automatic flight on the way, then when it completed the mission to fly over the 5 poles of the OHPL, it switched to RTL mode (Return To Land) - the color red, which forces the UAV to return from where it took off. The last flight mode used is MANUAL - yellow. It was used to land the UAV, as a protection measure against the rugged terrain specific to the area from which the flight was performed.

Fig. 4.10. The flight path executed by the designed UAV system

In addition to the selected flight modes, depending on the length of the segment specific to each point on the recorded route, you can see the difference in altitude in different phases of flight, and in fig. 4.11. there is an exact overlap of the orbits executed by the UAV system, above the high voltage poles, but also a precise maintenance of the flight altitude.

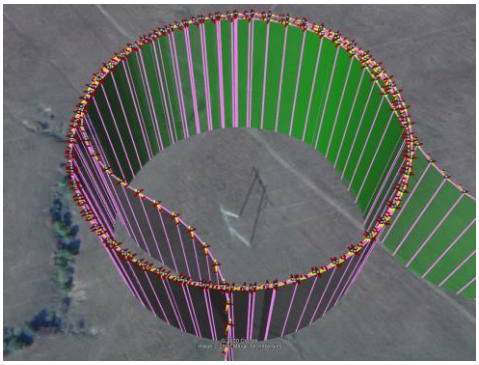

Fig. 4.11. Orbits over high voltage pole

IV.2. Experimental results obtained from the analysis of flight parameters

The analysis of the flight parameters verifies the veracity of the data from the flight sensors (accelerometer, gyroscope, magnetometer and barometer) so that the data injected in the calculation block of the distance to the target, which will be presented in the next chapter, is correct.

Also, the control components of the altitude control system based on the speed controller, calculated in the previous chapter, were integrated on autopilot, for experimental validation of numerical simulation, and the results are presented using graphs: engine speed vs. flight speed fig. 4.13 and engine speed vs altitude fig. 4.14. Also, an overall graph, comprising all the analyzed parameters underlying the altitude control and the stabilization of the longitudinal channel is presented in fig. 4.15.

Fig. 4.13. Electric motor speed vs flight speed

In fig. 4.13. the electric motor speed changes with the flight speed so that it remains as constant as possible. The variation of the flight speed shown in the graph is caused by the external factors represented by the wind speed on the y-axis.

Fig. 4.14. Electric motor speed vs altitude

In fig. 4.14. it is observed how the engine speed varies to keep the altitude constant, and when switching from AUTO flight mode to RTL flight mode, a speed reduction is observed for the UAV to decrease the altitude and enter the landing phase.

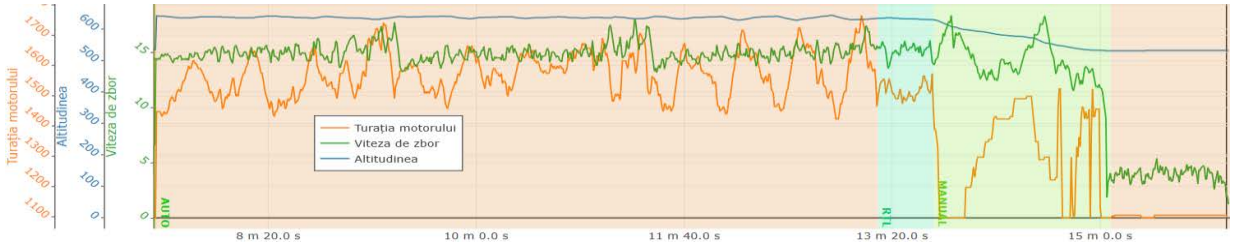

Fig. 4.15. Electric motor speed vs flight speed vs altitude

In fig. 4.15. the graph between engine speed, UAV speed relative to air grids and flight altitude is shown. It is clear that the speed controller works properly, because it varies the engine speed to keep the speed constant and implicitly the altitude that is analyzed in terms of errors in fig. 4.16, with minor errors that do not endanger flight safety.

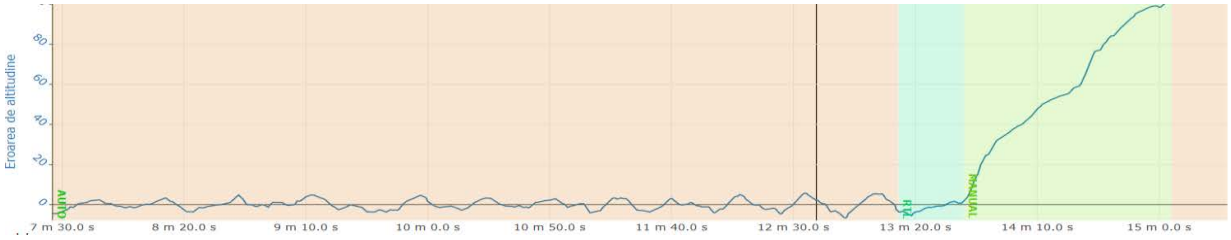

Fig. 4.16. Altitude error

Regarding the flight attitude of the UAV and the system's response to the commands received, figures 4.17, 4.18 and 4.19 show the errors, which are very small, referring to Euler's angles (attitude angles), namely, the angle of flight. roll, pitch angle and rotation angle. Thus, according to the graphs, the differences between the ordered angles and the angles executed by the UAV system are very small, which denotes a very good stability of the UAV during the flight on the way, as well as in the landing and take-off phases..

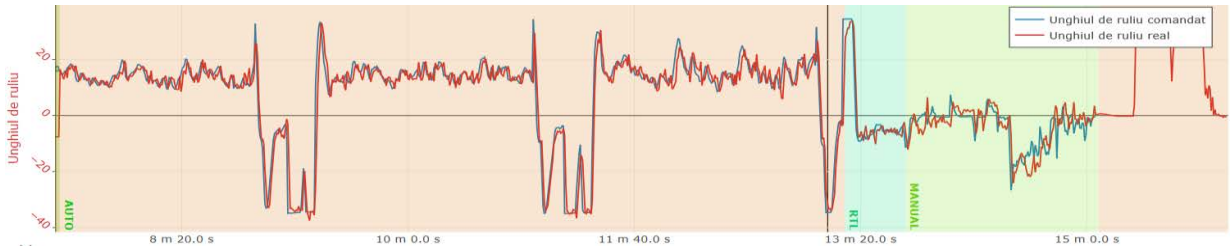

Fig. 4.17. Commanded roll angle vs real roll angle

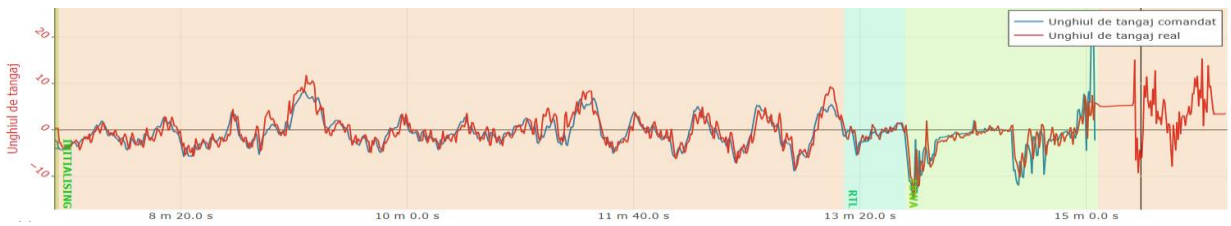

Fig. 4.18. Commanded pitch angle vs real pitch angle

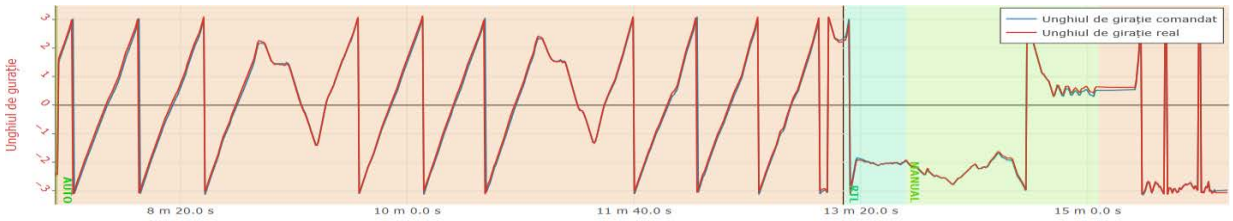

Fig. 4.19. Commanded yaw angle vs real yaw angle

In fig. 4.20. it is observed that the speed with respect to the ground given by the barometric sensor and the speed with respect to the air nets given by the Pitot tube which is connected to a differential pressure sensor, show great similarities and the small difference between them is caused by the speed of wind gusts and air currents.

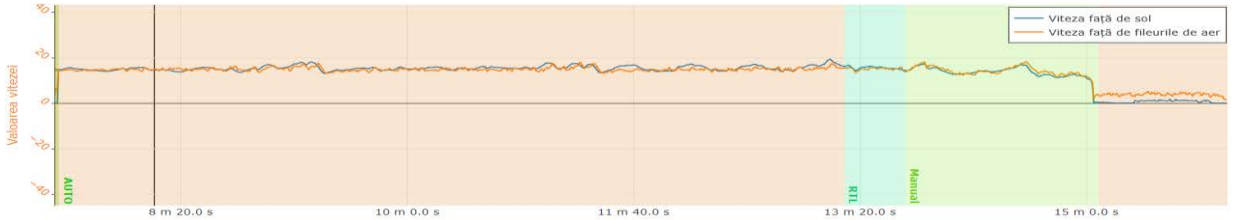

Fig. 4.20. Ground speed vs Pitot speed

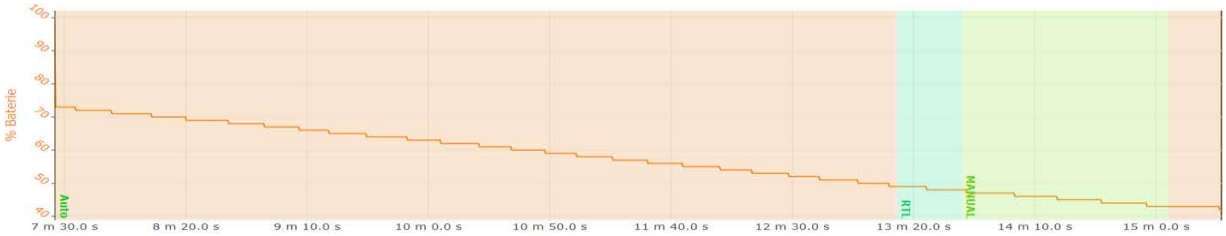

Fig. 4.21. Battery consumption rate

From the graph which shows the battery consumption rate, it can be concluded that the LIPO battery used to power the system decreased by 30% after 9 minutes of flight, making the system have a total flight range of approximately 30 minutes. Given that the flight was not intended to have a high flight range but only to demonstrate the stability of the UAV in the air, to improve flight endurance is considered the design of a UAV system with thermal engine, which can stay in the air over 10 hours.

From the analysis of UAV parameters and its behavior in case of a real flight on high voltage lines it can be stated that UAV systems with fixed wing are recommended for flight on OHPL, behave stably, sensors on board are not influenced by electromagnetic field of the line, so that this type of system does not endanger the physical integrity of the OHPL or the system operator.

In conclusion, the designed UAV system responded very well to the calibration tests, to the verification flight and, finally, to the overflight mission of a section consisting of 5 poles of the 400 kV high voltage power line, Brașov - Gutinaș, proving flight stability and operational safety.

V. ANALYSIS OF VIDEO DATA RECEIVED FROM UAV MOUNTED OPTICAL SENSOR

Real-time video processing based on data obtained from a Corona camera is the main objective of the flight, with the UAV system designed, on high voltage power lines. The video processing takes place on board the UAV, in real time and consists in processing, analyzing and classifying frame by frame extracted from the video signal provided by the optical sensor on board the UAV in order to identify the Corona discharge on the analyzed high voltage line. as well as its location for carrying out subsequent maintenance interventions. In fig.5.2. the block diagram of the video data stream at the body of the Sky Walker UAV system is presented:

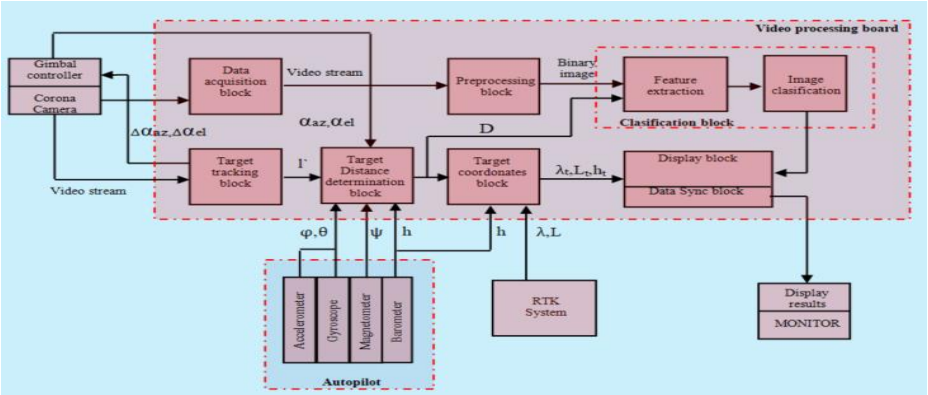

Fig. 5.2. Block diagram of CDC software

V.1. Data aquisition block

The data acquisition is done from the Corona camera mounted on board the UAV, then the signal is taken over by the data acquisition block, representing the first stage of the process of extracting the Corona discharge characteristics from a video stream. The video signal is transmitted from the camera to the processing board using the MIPI-CSI communication protocol that connects the video decoder attached to the camera to the Nvidia TX2 processing board running the CDC software.

To reduce computation time and streamline the designed algorithm, the raw video frame, extracted from the video stream delivered by the camera, is automatically converted to grayscale format.

In fig. 5.3. the transformation from a color image to a grayscale image using the brightness method is shown (Grayscale_pixel = 0.21 R + 0.72 G + 0.07 B).

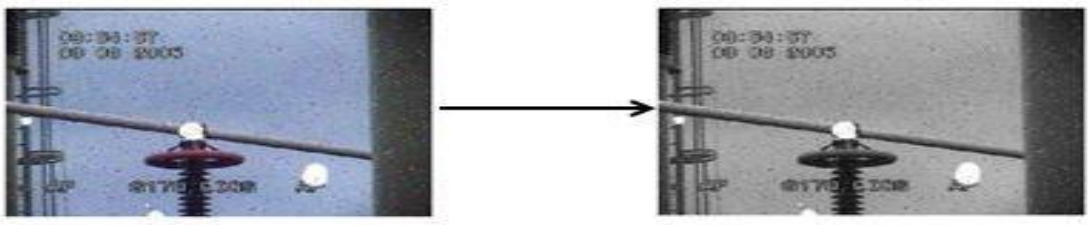

Fig. 5.3. Transform a color image to a grayscale image

Also, most image analysis and processing software uses the brightness method as a preset function.

V.2. Preprocessing block

In the preprocessing block, each video frame is analyzed to identify and isolate the pixels that may indicate the appearance of the Corona discharge. To achieve this isolation of the region of interest, a blur median filter [146] and a threshold filter were applied that reduce the image to pixel values of 0 and 1. Pixels indicate the background of the image. (ie black pixels), and with the value 1 are represented the pixels that indicate the Corona download in the image (white pixels).

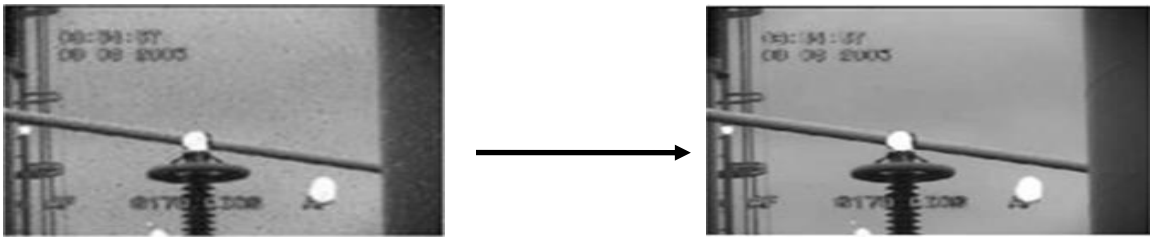

Fig. 5.4. Apply a 3x3 kernel to eliminate noise

By applying a mask (kernel) over the processed image and with the help of convolution algorithms can substantially improve an image so that the extraction of features of interest, ie white pixels in the image indicating the existence of Corona download can be executed much easier. In fig. 5.4. an improved image is presented, on which a 3x3 size kernel was applied [148].

Regarding the transformation from a grayscale image to a binary one, a lower limit (a threshold value) of 250 was chosen, ie any pixel value less than 250 becomes a black pixel (value of 0). This value was chosen after several attempts, because it is not desired that the gray pixels in the image (with values less than 250) be identified with the specific pixels of the Corona discharge, but it was also considered that the Corona discharge cannot be represented by perfectly white pixels (with a value of exactly 256), because there is no perfect white in a frame of nature.

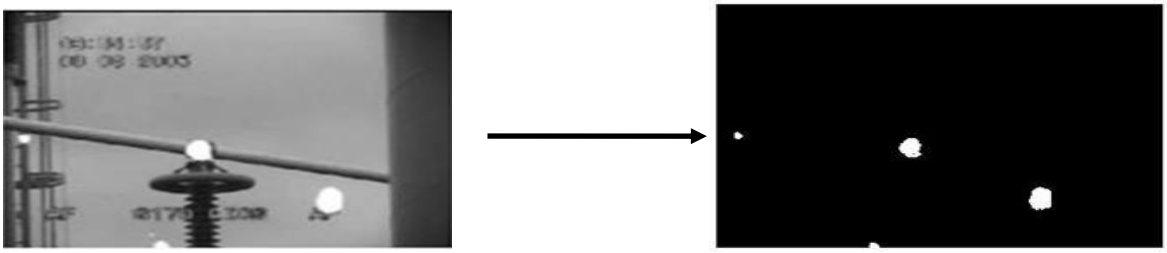

Fig. 5.5. Binary image resulting from the segmentation process

Figure 5.5 shows the transition from an enhanced grayscale image to a segmented image to which a threshold value of 250 has been applied. The main reason that led to the use of the 2 image processing methods: median filter and dash method is justified by the fact that the white spots that appear in the image, identified as Corona discharge, are difficult to determine and then can not be identified as an object.

V.3. Target distance calculation block

In order to increase the accuracy when determining the volume of white pixels in the image, and the existence of air ionization around the conductor to be correctly estimated, it is necessary to know, in real time, the distance from the optical sensor on the UAV and the target of interest, manually selected by at the ground control station, represented by the electrical conductor subjected to Corona discharge.

The first step in determining the distance between the UAV and the place of occurrence of the Corona discharge is to establish a link between the coordinate systems of the UAV and the coordinate systems connected to the optical sensor.

Figure 5.8 shows the relationship between the inertial coordinate system, the coordinate system rigidly connected to the UAV and the coordinate system related to the camera stabilization system (gimbal). Therefore, in order to switch from the UAV body-frame system coordinate system to the coordinate system connected to the optical sensor or camera, 3 intermediate switching coordinate systems must be considered: Sg1 = (xg1, yg1, zg1), Sg = (xg , yg, zg), Sc = (xc, yc, zc), where Sc represents the coordinate system of the camera.

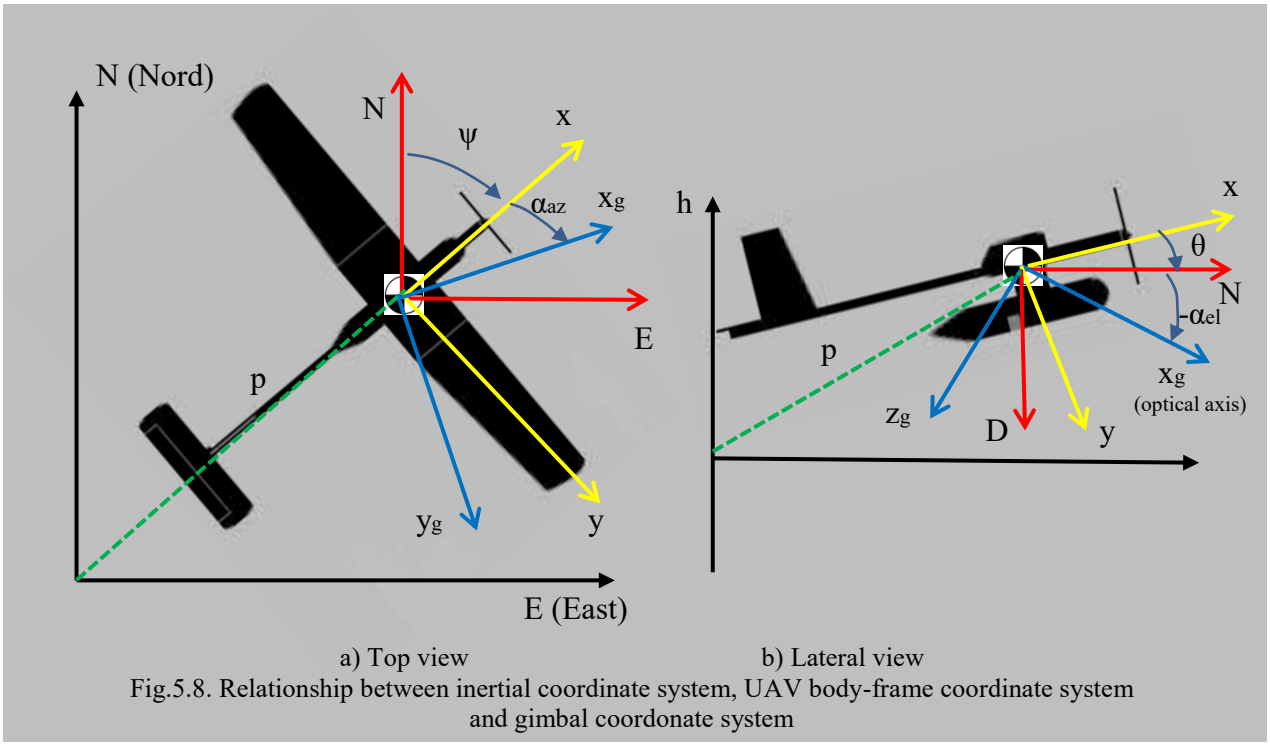

a) Top view b) Lateral view

Fig.5.8. Relationship between inertial coordinate system, UAV body-frame coordinate system and gimbal coordonate system

A coordinate system is transformed into another coordinate system using two basic operations: rotation and translation.

Knowledge of the rotation matrices that shape the transition from the Earth-related coordinate system (inertial), to which the coordinates of the GPS / RTK system are related, to the UAV body-frame system coordinate system, in which the attitude angles of the UAV are represented, or to the coordinate system of the gimbal in which the position of the Corona camera is represented, is necessary for the transmission and fusion of data between the calculation blocks.

V.3.1. Mathematical model of the optical sensor (Corona camera)

In order to be able to use high capacity image processing it is necessary to determine the mathematical model of the optical sensor (Corona camera). Also, knowing the technical characteristics of the camera plays an important role in determining the Corona discharge by processing the received video stream.

In figure 5.9. the coordinate system of the camera is presented. Therefore, in the case of flying on high voltage lines, the target is represented by the Corona discharge, so implicitly by the area of the insulators arranged at the base of the pillar crown. For future calculations the target will be denoted by lt. The projection of the target in the image plane is denoted by p. The location of the pixels with coordinates (0,0) corresponds to the center of the image and must be aligned with the optical axis of the camera. The distance to the target is denoted by D and is measured in meters.

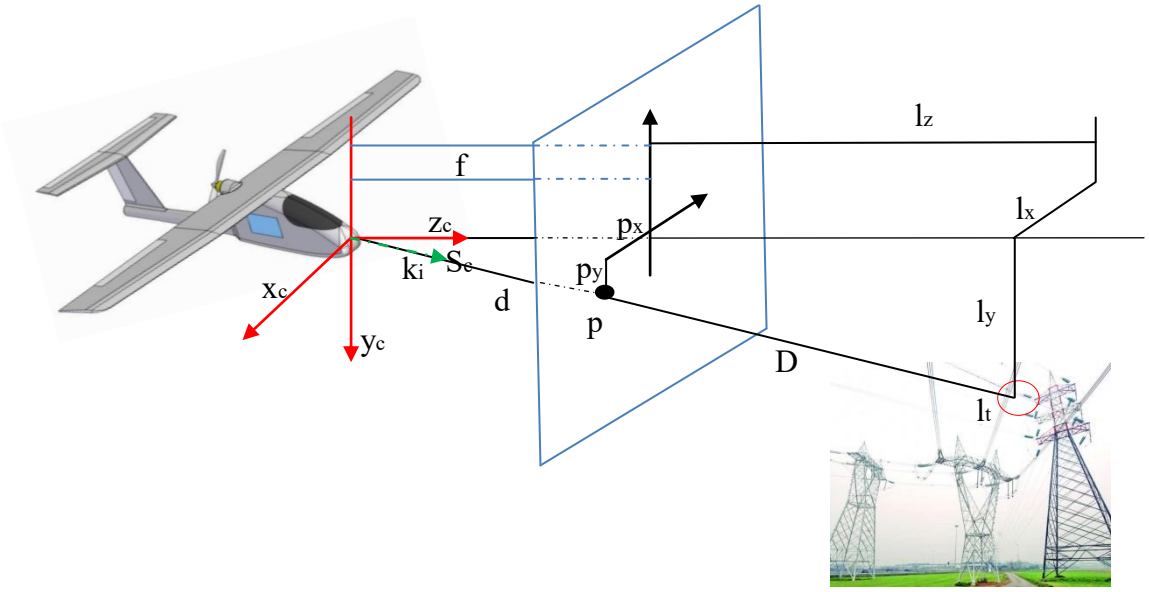

Fig.5.9. Mathematical model of the optical sensor

From geometry, the following relation results which describes the position of the target of interest in inertial coordinates as follows :

$$p_{st}^{i} = p_{UAV}^{i} + R_{\Psi\Theta\Phi} R_{\Psi\Theta\Phi}^{g} R_{g}^{c} l_{c} \quad = p_{UAV}^{i} + D(R_{\Psi\Theta\Phi} R_{\Psi\Theta\Phi}^{g} R_{g}^{c} l') \tag{5.3.41}$$

Where: $p_{UAV}^{i} = (p_n, p_e, p_d)^T$

$R_{\Psi\Theta\Phi} = R_{\Psi\Theta\Phi} = [R_\Psi][R_\Theta][R_\Phi]$

$R_{\Psi\Theta\Phi}^{g} = R_{\Psi\Theta\Phi}^{g}(\alpha_{az}, \alpha_{el})$

The Flat Earth Model method was used to determine this distance. Figure 5.9 shows a method of estimating the distance to the target assuming that the Earth is flat, ie the relief is not uneven.

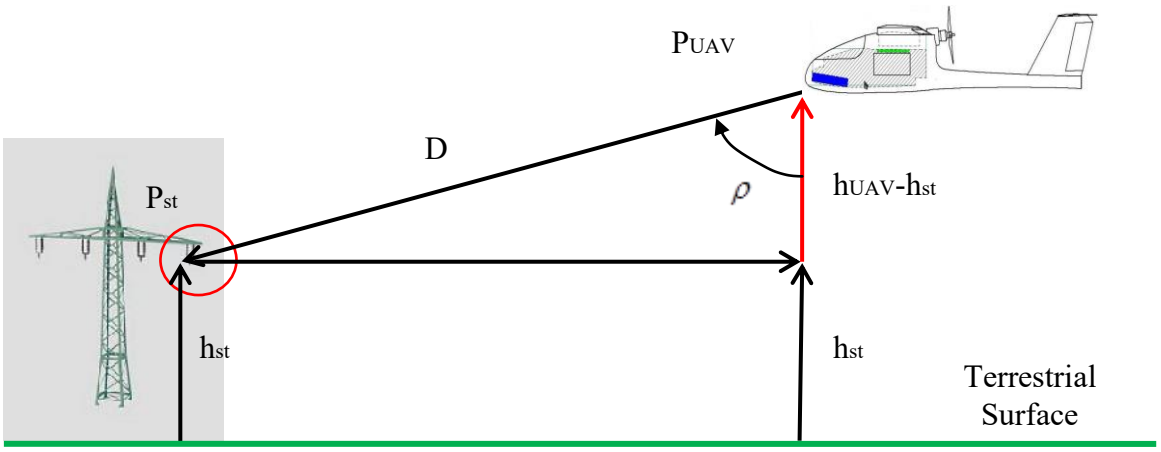

Fig.5.10. Estimation of the distance to the target using the Flat Earth method

Using this method the following notations can be made: $h_{UAV} = -p_d$ it is AGL altitude of the UAV and ρ is the angle between l (the vector of the relative position between the pole of interest and the UAV) and the z axis of the inertial coordinate system.

From Figure 5.10 the following relation can be deduced:

$$D = \frac{h_{UAV} - h_{st}}{\cos\rho} \tag{5.3.42}$$

Where : $\cos\rho = k_i * l' = k_i * R_{\Psi\Theta\Phi} R^g_{\Psi\Theta\Phi} R^c_g l_c$

k_i - the direction vector of the target

In conclusion, the estimated distance to the target using the Flat Earth model is s follows:

$$D = \frac{h_{UAV} - h_{st}}{k_i * R_{\Psi\Theta\Phi} R^g_{\Psi\Theta\Phi} R^c_g l_c} \tag{5.3.43}$$

Determining the target distance is one of the important achievements of this work, and for further developments this parameter is essential in determining estimates of the level of losses caused by the Crorona discharge over a certain lenght of a section of overhead power line.

V.4. Target coordinate calculation block

This section presents a method for determining where the Corona discharge takes place in the Earth-related (inertial) coordinate system assuming that a Corona camera mounted on a stabilization system (gimbal) is used, both of which are integrated aboard a fixed wing UAV. It is assumed that the UAV is able to measure its inertial coordinates on its own, with the help of the RTK (Real Time Kinematics) system integrated on board and which increases the accuracy to the order of centimeters unlike an ordinary GPS system.

Knowing the distance to the target, the position coordinates in the inertial system of the Corona discharge can be calculated using the following equation:

$$p_{st}^{i} = \begin{bmatrix} p_n \\ p_e \\ p_d \end{bmatrix} + (h_{UAV} - h_{st}) \frac{R_{\Psi\Theta\Phi} R^{g}_{\Psi\Theta\Phi} R^{c}_{g} l'}{k_i * R_{\Psi\Theta\Phi} R^{g}_{\Psi\Theta\Phi} R^{c}_{g} l_c} \quad (5.4.44)$$

By determining the coordinates of the target of interest, namely the Corona discharge, newreserch topics are open regarding the creation of a map with the areas where the Corona discharge was detected, thus facilitating the intervantion of maintenance teams to remedy the defects that cause this phenomenon.

V.5. Target tracking block

Tracking the Corona discharge by the optical sensor, when it is discovered, is an essential step in the video signal analysis process. The classification of the Corona discharge is made according to the number of relevant pixels (white pixels) in the image, which requires a stable and permanent follow-up of this phenomenon.

As shown in the block diagram of the CDC software (fig. 5.2), the target tracking block processes the video signal received from the Corona Camera or any other video source on board the UAV. This block, based on the received signal, calculates the deviations of the attitude angles of the gimbal (camera stabilization system), so that the pixel coordinates of the selected target overlap with the coordinates of the image center, so that, regardless of the evolution of the UAV, the target does not disappear. the video frame, moreover, should always remain in the center of the image.

V.5.1. Calculation of the gimbal angle corrections

Small UAV systems are used, as is the case with the UAV designed, most often, to perform ISR (Intelligence Surveillance Reconaissance) missions. If the UAV is equipped with a camera stabilization system (gimbal), this involves control over the camera so as to focus on the targets.

The gimbal used for flight over the OHPL is designed on 2 axes (azimuth and elevation), which means that the equations of motion for the gimbal assembly are:

$$\dot{\alpha}_{az} = \Delta\alpha_{az} \quad (5.5.45)$$

$$\dot{\alpha}_{el} = \Delta\alpha_{el} \quad (5.5.46)$$

Where : $\Delta\alpha_{az}$ and $\Delta\alpha_{el}$ are the control variables of the azimuth angles and the elevation of the gimbalm respectively.

The next step is to determine the azimuth and elevation angles taking into account that, in a video frame extracted from the video stream, the optical axis is given by the vector $(0,0,1)^c$. Thus, following the processing of the video signal and the application of tracking algorithms, the commanded azimuth and elevation angles are generated $\left(\alpha^c_{az}, \alpha^c_{el}\right)$.

Result:

$$\tilde{l}_d^{UAV} = \begin{pmatrix} \tilde{l}_{xd}^{UAV} \\ \tilde{l}_{yd}^{UAV} \\ \tilde{l}_{zd}^{UAV} \end{pmatrix} = R_g^{UAV}(\alpha_{az}^c, \alpha_{el}^c) * R_c^g \begin{pmatrix} 0 \\ 0 \\ 1 \end{pmatrix} = \tag{5.5.51}$$

$$= \begin{pmatrix} \cos\alpha_{el}^c \cos\alpha_{az}^c & -\sin\alpha_{el}^c & -\sin\alpha_{el}^c \cos\alpha_{az}^c \\ \cos\alpha_{el}^c \sin\alpha_{az}^c & \cos\alpha_{az}^c & -\sin\alpha_{el}^c \sin\alpha_{az}^c \\ \sin\alpha_{el}^c & 0 & \cos\alpha_{el}^c \end{pmatrix} \begin{pmatrix} 0 & 0 & 1 \\ 1 & 0 & 0 \\ 0 & 1 & 0 \end{pmatrix} \begin{pmatrix} 0 \\ 0 \\ 1 \end{pmatrix} = \begin{pmatrix} \cos\alpha_{el}^c \cos\alpha_{az}^c \\ \cos\alpha_{el}^c \sin\alpha_{az}^c \\ \sin\alpha_{el}^c \end{pmatrix}$$

By determinating the commanded azimuth and elevation angles α_{az}^c si α_{el}^c the desired azimuth and elevation angles can be determinated:

$$\alpha_{az}^c = tg^{-1}\left(\frac{\tilde{l}_{yd}^{UAV}}{\tilde{l}_{xd}^{UAV}}\right) \tag{5.5.52}$$

$$\alpha_{el}^c = \sin^{-1}\left(\tilde{l}_{zd}^{UAV}\right) \tag{5.5.53}$$

In conclusion, the correction commands of the servomechanisms that operate the gimbal can be defined as follows:

$$\begin{aligned} \Delta\alpha_{az} &= k_{az}(\alpha_{az}^c - \alpha_{az}) \\ \Delta\alpha_{el} &= k_{el}(\alpha_{el}^c - \alpha_{el}) \end{aligned} \tag{5.5.54}$$

Where k_{az} and k_{el} are the gain values of the gimbal PD control system.

Deviations from the center of the image determined by equations (5.5.54) are transmitted to the gyro-stabilized platform to compensate for target tracking errors.

At the moment of implementing the mathematical calculation regarding the determination of the correction commands, then the ground operator of the UAV, is able to command the stopping of the video transmission from the monitor of the control station. the isolator where the Corona discharge was identified).

The selection of the target of interest can be made by means of points or a geometric shape of square, rectangle, circle or ellipse type, fig. 5.12.

Fig.5.11. The frame selected at the time of stopping of video transmission

Fig.5.12. Tracking the target of interest

Because the tracking algorithm used only uses the shade of the HSV (Hue Saturation Value) color space and ignores pixels with high or low brightness, the system offers a high tolerance to illumination. As long as the occlusion of the target is not 100%, what is left of the target probability distribution will be tracked. The search window will change its size according to the size of the target, automatically managing the irregularities induced by its movement.

V.6. Classification block

The classification block contains the classes and methods needed to make a prediction based on more data than simply the number of white pixels remaining in a binary image. For the classification of binary images, a series of methods were chosen to be implemented, the best known in the field, so as to create a basis for comparison in order to continue the study. For a more efficient classification, it was decided to analyze several algorithms specific to machine learning domain.

V.6.1. Description of the machine learning algorithms under analysis

For an overview of the types of existing algorithms and choosing the most suitable one for the Corona discharge classification, in this section a study was made on the processing characteristics and the mathematical model behind several machine learning algorithms.

Next, several supervised learning algorithms are presented, based on which the obtained data sets will be processed later.

V.6.1.1. SVM algorithm (Support Vector Machine)

Mathematically, a supervised machine learning algorithm that uses SVM can be described by the equation of the hyperplane as follows:

$$f(x) = \alpha x' + b = 0 \tag{5.5.55}$$

Where, α and b are real numbers, and setting these numbers so that $||\alpha||$ they are minimal for all data points (x_i,y_i), where $y_i f(x_i) \geq 1$.

For this values, x_i, which is at the edge of the separation plan, $y_i f(x_i)=1$.

It is necessary to know that the data sets are in fact sets of points (vectors), x_i, associated with categories, y_i, for different sizes, d, where $x_i \in R^d$ and $y_i = \pm 1$.

Therefore, the optimal solution for the quadratic programming problem is given by the pair $(\hat{\alpha},\hat{b})$, which classifies the vector z according to the equation:

$$clasă(z) = sign(z'\hat{\alpha} + \hat{b}) = sign(\hat{f}(z)) \tag{5.5.56}$$

Where, $\hat{f}(z)$ represents the classification score and z is the distance between the separation hyperplane and the margin.

To increase the size ofthe distance from the hyperplane to the separation margin, use the kernel function.

V.6.1.2. Classification linear algorithm

Determining the standard parameters for a linear classification algorithm involves solving an optimization problem, as defines as follows [156]:

$$\min(w)\frac{1}{2}w^T w + C\sum_{i=1}^{l}\xi(w;y_i,x_i) \tag{5.5.57}$$

Where C is the regularization parameter and $\xi(w; y_i, x_i)$ it is the loss function that is defined as such:

$$\xi(w; y_i, x_i) = \begin{cases} \max(0, 1 - yw^T x) \\ \max(0, 1 - yw^T x)^2 \\ \log(1 + e^{-yw^T x}) \end{cases} \quad (5.5.57)$$

In equation (5.5.57), the first branch of the loss function is called the degree 1 loss function, the second branch is called the degree 2 loss function, and the third branch is the logarithmic loss function.

V.6.1.3. Linear kernel algorithm

The main difference between a linear classification algorithm and a linear kernel classification algorithm is that each vector is mapped as in a different dimensional space. For example, as a function of degree 1 losses in equation (5.5.57), it becomes:

$$\max(0, 1 - y_i(w^T \phi(x_i) + b) \quad (5.5.58)$$

Where b is the bias term.

Usually, $\phi(x)$ has a very large size, and for this reason calculation methods based on the feature space (*KT – Kernel Tricks*) are applied [158]. So, w, become a linear combination of $\phi(x_i)$, $\forall i$:

$$w = \sum_{i=1}^{l} y_i \alpha_i \phi(x_i) \quad (5.5.59)$$

Where α_i, $\forall i$ are the solutions to the following optimization problem:

$$\min_\alpha \frac{1}{2} \alpha^T Q \alpha - e^T \alpha, \; 0 \le \alpha_i \le C, \forall i, \; y^T \alpha = 0 \quad (5.5.59)$$

Where $Q_{ij} = y_i y_j K(x_i, x_j)$, $K(x_i, x_j)$ being a kernel function, while e it is the vector with values of 1.

For the other 2 functions of equation (5.5.57), the degree 2 loss function and the logarithmic loss function, the optimization problem is presented in references [159] and [160].

Polynomial kernel and Gaussian kernel classification algorithms, also called Radial Base Function (RBF), are also often used.

V.6.1.4. Polynomial kernel algorithm

In the analysis performed by the determination of the best classification algorithm suitable for determining the Corona discharge, the classification algorithm with polynomial kernel was studied. So, mathematically, it can be defined like this:

$$K(x_i, x_j) = (\gamma x_i^T x_j + r)^d \quad (5.5.60)$$

Where γ and $r > 0$, and d it is the parameter that gives the degree of the polynomial, this being established by the operator.

V.6.1.5. RBF – Radial Base Function algorithm

To use a Gaussian-type classification algorithm or radial-based function, an infinite dimension is considered. In such a space, the data set must necessarily be separable. This implies greater complexity and computational time, but in this way the separation of data is ensured and the categories of data are determined more accurately.

The kernel with radial base function is one of the most known and used kernels, being described by the following equation:

$$K(x_i, x_j) = e^{-\gamma \|x_i - x_j\|^2} \tag{5.5.61}$$

One of the best known guidelines for applying SVM classification algorithms suggests the following steps to drive a linear kernel classification algorithm: 1. Labeling of each characteristic, of the video frames used for training, on the interval [-1, + 1]; 2. Using a Gaussian kernel and selecting the parameters C and γ, which give the most accurate results to the cross-validation method (CV); 3. Obtaining the model w based on parameters C and γ.

V.6.1.6. Kernel algorithm with logistic regression

Assumptions can greatly simplify the learning process, but they can also limit what can be learned. Algorithms that simplify the function in a known form are called parametric machine learning algorithms. One of the classification algorithms based on parametric algorithms is the logistic regression kernel classification algorithm. Such an algorithm can be expressed mathematically according to the following equation [161]:

$$P(Y = 1 \mid x, w) = \frac{1}{1 + e^{-(w \cdot \phi(x) + b)}} \tag{5.5.61}$$

Next, the weight function are defined, w, as such support vectors:

$$P(Y = 1 \mid x, w) = \frac{1}{1 + e^{-(\sum_i \alpha_i \phi(x_i) \cdot \phi(x) + b)}} \tag{5.5.62}$$

Eventually it was written that way:

$$P(Y = 1 \mid x, w) = \frac{1}{1 + e^{-(\sum_i \alpha_i K(x, x_i) + b)}} \tag{5.5.63}$$

Equation (5.5.63) is the mathematical support behind a logistic regression kernel clasification algorithm.

V.6.1.7. kNN (k – Nearest Neighbor) algorithm

The set of algorithms for classification by the kNN method is based on the central idea that the closest data points (neighbors) in a certain class can choose the class of the example on which the classification is made. For example, if you analyze a set of 5 video frames, and 3 of them are classified as images in which the Corona discharge appears, and 2 show nothing, then it means that the group they belong to will be classified as a metadata in which Corona discharge appears.

V.6.1.8. RadiusNN (Radius Nearest Neighbor) algorithm

The principle behind the methods based on the nearest neighbor is to find a predefined number of training samples that are closest to the new point analyzed and to predict its labeling. The number of samples can be a user-defined constant (k - nearest neighbors) or varies depending on the local density of points (nearest neighbor depending on radius - RadiusNN). Distance can generally be any metric measure, so standard distance, Euclidean, is the most common choice.

Despite its simplicity, this classification algorithm has enjoyed success in a large number of classification and regression problems, including handwritten figures or satellite imagery. Being a non-parametric method, it is often used successfully in classification situations where the separation plan is very irregular.

V.7. Results storage and display block

Finally, the block of storage and display of results is what can be called the human-machine interface and the place where all measured data is analyzed and where they are transformed into significant results. The proposal for this module is a graphical interface (GUI) in which the video stream is played back on the screen, and on the same screen are attached the metadata extracted from the processing and classification of the analyzed frames. The operator may take this into account in determining decisions regarding the continuation of the flight mission.

VI. FINAL EXPERIMENTAL RESULTS

This chapter presents the results obtained after the analysis of supervised machine learning algorithms and their response in order to identify the Corona discharge from the test data package used.

For the analysis of the performances of these algorithms, the metrics used are the execution time and the obtained score. The evaluation was performed using the CV (Cross Validation) method.

VI.1. Methods of validating the results

Interpretation of results is one of the most important activities in identifying Corona download, thus validating the work done in developing the designed CDC software. In order to be sure that the results are plausible and correspond to the requirements proposed from the beginning, two evaluation methods were used.

The following is how to interpret the results based on the cross-validation method.

In order not to reduce the final amount of data by dividing it into several sets, the Cross Validation (CV) method was used, with which the test data set was abandoned, dividing the data set only into training data and training data validation.

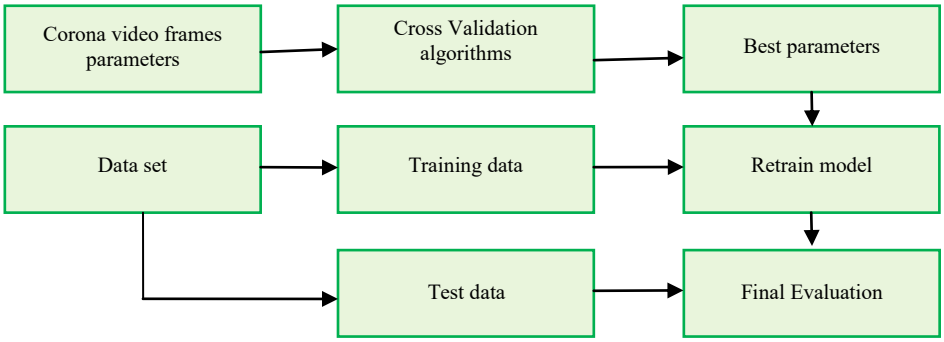

Fig. 6.1. Working diagram of the cross-validation (CV) algorithm

The cross-validation methos involves 2 possible approaches: (1) cross-validation with division into mini-data sets (K-fold) and (2) cross-validation with random division of data sets (ShuffleSplit).

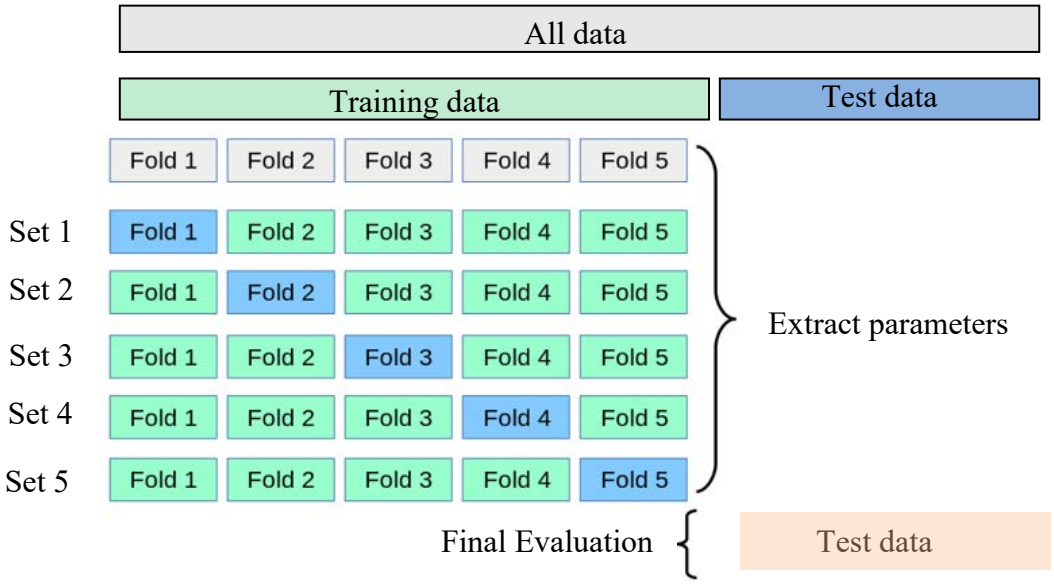

Fig. 6.2. K-fold cross-validation method operation diagram [162]

In the basic approach, called K-fold cross-validation, the training set is divided into smaller k sets (folds), as shown in Figure 6.2.

In figure 6.3. the data behavior of the K-fold cross-validation method is presented, specifying that this method is not influenced by classes or groups of data.

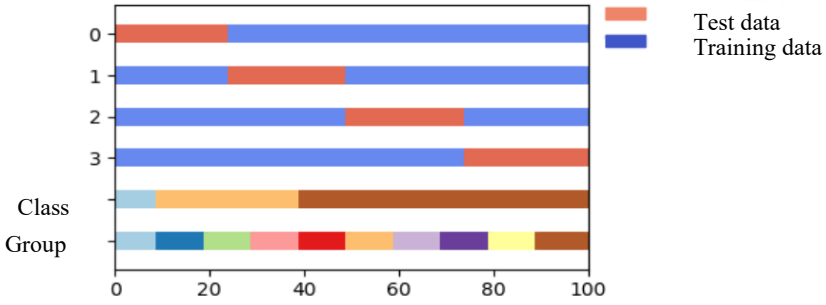

Fig. 6.3. K-fold cross-validation method [162]

The cross-validation method with random division of data sets (ShuffleSplit) is based on random permutations of data sets which in this case are divided into sets even smaller than

the K-fold method. Thus, the iterator of this validation method generates a user-defined number of independent training or test instances, respectively.

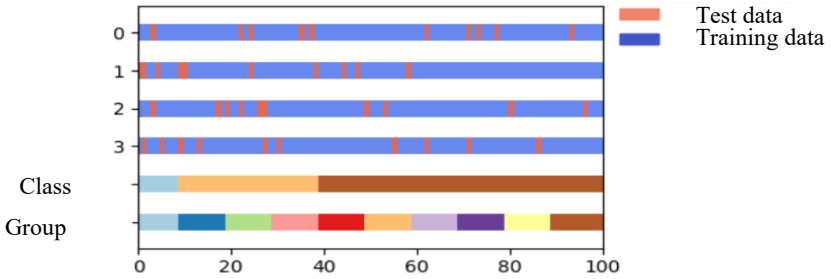

Fig. 6.4. ShuffleSplit cross-validation method [162]

The cross-validation method with random division of data sets (ShuffleSplit) is a good alternative to cross-validation with division into data minisets (K-fold), therefore, both methods were used in the analysis of Corona download classification algorithms. Thus, it can be stated that the results obtained have double validation.

VI.2. Data sets description

The preparation of the video data for the classification precess was a challenge and at the same time a satisfaction as it was possible to acquire 4 different data sets, each set representing a Corona discharge souce.

The first set of data is represented by a collage, processed and resized, consisting of various video sources, without restrictions of intellectual property rights (eng: open source), in which the Corona discharge appears. Concluding that more training data is needed for the classification algorithm to be as accurate as possible, the second set of data was obtained in the laboratory, by purchasing video frames from a Corona generator, set at different intensities. The third data set was obtained by replacing the electric arc produced by the Corona discharge with an electric arc produced by welding, forming pixels with light intensity above the threshold value of 250. This made the data set number 3 not as efficient as I thought.

For the testing of the Corona discharge detection and classification algorithm, as a test data set, the videos recorded following the verification flight of the designed UAV system were used, just above the 400 kV high voltage line, Brașov-Gutinaș.

In fig. 6.5 presents the four data sets used to drive and test the Corona discharge classification algorithms.

For the uniformity of the input data and taking into account the image resolutions used as output data by some of the most popular Corona cameras, all data sets have been converted to a resolution of 320x240 pixels. This, in addition to the decision to transform the images into grayscale format, led to an increase in computational speed and thus to an increase in the scores that characterize the accuracy of the classification algorithms.

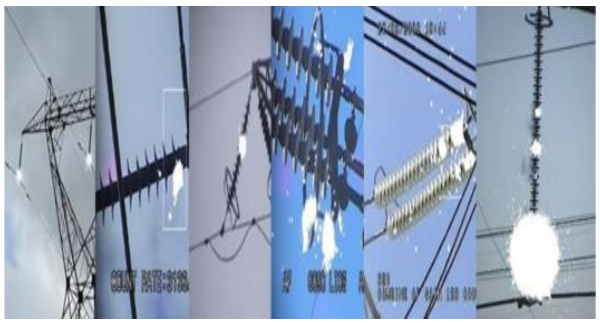

a) Collage with open source videos (Data Set 1)

b) Laboratory generated Corona discharge (Data Set 2)

c) Sumulated arc Corona discharge – welding (Data Set 3)

d) Processing of flight video recordings on high voltage lines (Data Set 4)

Fig. 6.5. Description of the data sets used to drive and test the classification algorithms

VI.3. Experimental results obtained

In order to demonstrate the choice of the best supervised machine learning algorithm, following the conparison of a number of 8 algorithm, their analysis was carried out during a number of 4 experiments approached in stages.

In the first phase, the acquisition, critical analysis and transformation of the first data set was performed, from a number of open source videos into a video collage that can be used to improve the developed algorithm. This first data set was mainly used to justify the functionality of the preprocessing module, proving that the choice of the procedure for filtering video frames with a median filter was an inspired choice.

VI.3.1. Experiment I – Demonstration of the usefulness of the preprocessing module

Starting from the formulation of the problem, namely, that the pattern of Corona discharge manifestation is unpredictable and difficult to model as a representation in an image, the first experiment aims to choose the optimal methods of preprocessing video frames received from the UV sensor on board UAV- so that the selected characteristics are representative of the classification problem.

For a more varied experiment, in each instance of the data set used, before dividing into „training data", respectively, "test data", a random combination of samples was performed.

The 2 comparative graphs below were produced in order to demonstrate the significant difference between the two levels of filtering the input image in terms of the scores obtained. In

this chosen scenario, it can be seen how the results increase significantly, in the case of all analyzed algorithms the score increases, and in terms of data accuracy, SVC algorithms with RBF kernel, KNN and KNN radius also show a significant increase.

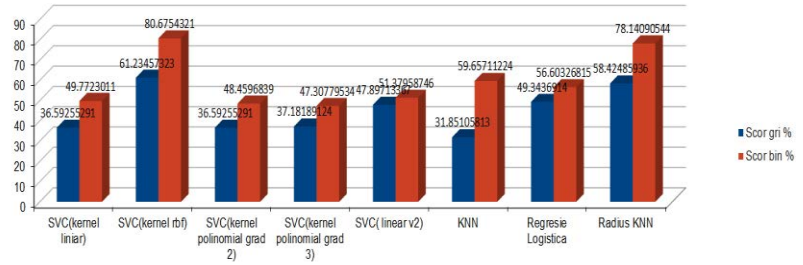

Fig. 6.8. Comparative score of grayscale data set vs binary data set

Figure 6.8 shows an increase in the score of binary data by 19.44% compared to grayscale data, in the case of the SVC algorithm with RBF kernel, in the case of the Radius KNN algorithm, the percentage increase is 19.72%, and in the case of the algorithm, KNN , the increase is even higher, reaching a percentage of 27.80%.

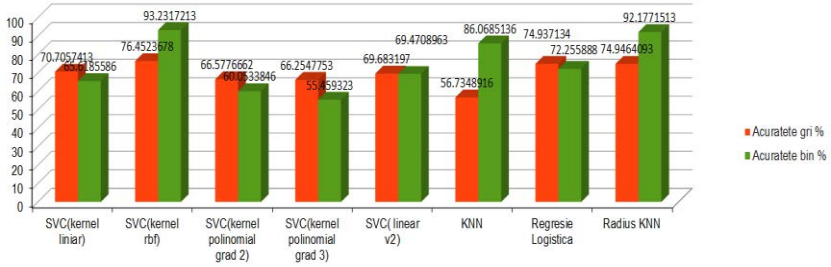

Fig. 6.9. Comparative accuracy of grayscale data set vs binary data set

In the case of the accuracy of the algorithms on the analyzed data sets, it can be seen in Figure 6.9 that the algorithms that best responded to the analysis of the comparative score between the gray data set and the binary data set also had a superior accuracy. In the case of SVC algorithms with RBF kernel the increase was 16.78%, and in the case of the Radius KNN algorithm, the increase was 17.92%, while for the KNN classification algorithm, the increase was even higher, reaching up to at 29.33%.

In conclusion, it can be seen that after applying the threshold method and segmenting the images, resulting in binary images, both the score and the accuracy of the classification algorithms increase from 10% to 30%.

VI.3.2. Experiment II – Empirical testing of possible algorithms

For experiment number II, to the data set number 1, another data set is added (data set number 2), obtained experimentally in the laboratory and consisting of a number of approximately 1000 video frames representing images recorded by the Corona PCO camera. Ultraviolet on a Corona discharge generating installation.

Also, the proposed experimental method is based on the cross-validation method by checking with the two data sharing approaches, presented in section VI.1, namely the K-fold cross-validation method (the total amount of data is divided into 5 sets) and the ShuffleSplit cross-validation method (the total amount of data is divided into n random sets). To avoid overfitting, the total data set was divided into training data (70%) and validation data (30%).

Figure 6.11 shows the comparative evolution of training times and test times for each algorithm. Therefore, it is observed that, for example, for one of the analyzed classification algorithms that performed well in previous verifications, namely the RadiusNN algorithm, the test time is slightly longer than the time of the other algorithms. This is explained by the need to learn a new test, which is different from the tests already introduced in modeling.

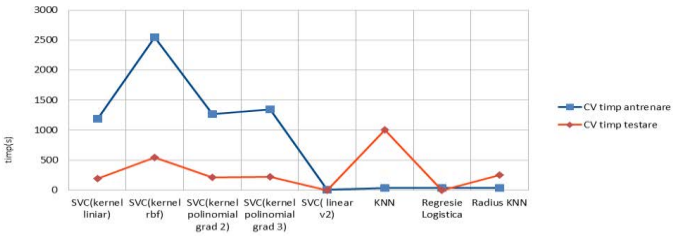

Fig. 6.11. Representation of training times and testing of the analysed algorithms

From the analysis of the results of Experiment II, it can be concluded that the introduction of new data sets considerably improves the results obtained. This aspect was the basis for the acquisition of data set number 3, the Corona discharge simulated by an electric arc welding.

The following graph shows a comparative analysis of the evolution of the classification algorithm score under analysis for the 3 variants run in the experiments: (1) grayscale images, (2) binary images (threshold method) and (3) extension data set. For uniformity, all results are presented using as a metric, the score, the accuracy metric being excluded.

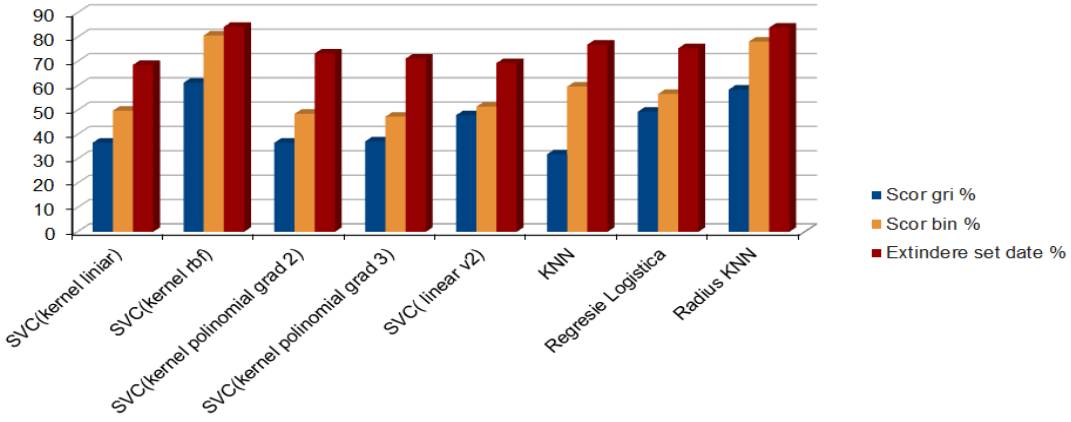

Fig. 6.13. Results after training the algorithms with the data set 2

Figure 6.13 is the most eloquent for experiment II, as an increase in the scores of all algorithms is observed. There is also a gradual increase in each algorithm, for example, linear kernel SVC has a score percentage of 36.59% after training with a set of grayscale images, after training with a set of binary images the percentage increases to 49.77%, ie by 13.18%, and when using the second data set the score increases by 31.98% compared to the training score with grayscale images.

VI.3.3. Experiment III – Optimization of chosen algorithms

In the case of experiment III for Corona image processing, the optimization of the basic parameters of the analyzed classification algorithms was performed, using the GridSearchCV method, specific to the Python Scikit software package. With this method you can check a series of values for standard parameters, such as C, gamma (γ) and the number of neighbors, returning the best parameterized estimator after running 5 times the database provided

The results of running the new parameters chosen by the GridSearchCV method are presented in figure 6.14, having as validation metrics: (1) the average score for dividing the complete data set into 5 subsets (folds), (2) the validation score after choosing the parameters and (3) the test score on a data set at first glance. All score metrics are represented as a percentage.

For a more concrete example of the results, the best 3 classification algorithms were chosen, 2 that had consistently good results over the previous experiments, namely SVC with RBF and Radius NN kernel and a third algorithm with initially poor results, SVC with linear kernel. The purpose of choosing the third weakest algorithm is to follow the extent to which the optimal choice of some parameters can lead to clearly superior results. It can be seen below that, although it initially showed poor results, during the experiments the performance increased considerably, reaching a percentage of 82.84% following the optimizations.

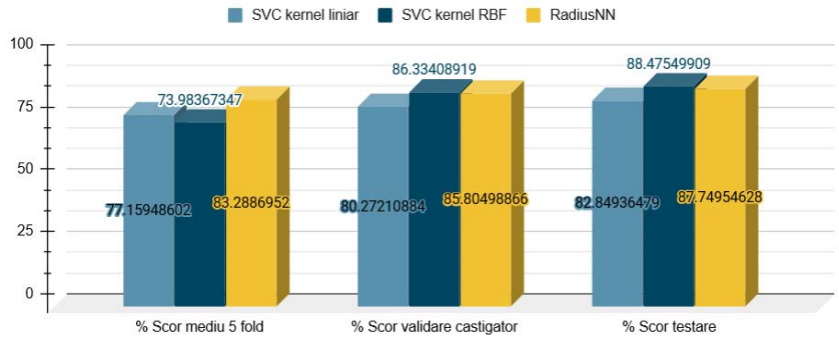

Fig. 6.14. Graphical representation of the scores of the schosen algorithms

Figure 6.14 shows the new scores obtained after optimization with the GridSearchCV method. A first observation is directed to the linear kernel SVC algorithm which has spectacular increases in the results obtained. Thus, based on the cross-validation method K-Fold with 5 layers obtains an average score of 77.16%, the winning score between the 5 iterations being 80.27%. Following the same type of progression as the other algorithms in experiment III, the test results on 20% of the remaining data increase to 82.84%. The same thing happened with the other 2 chosen algorithms, with a percentage increase of 19.58%, in the case of the SVC algorithm with RBF kernel, and in the case of the RadiusNN algorithm, the increase was only 2.26%. This relatively small increase for RadiusNN may suggest that the model is already at a saturation level that is no longer sensitive to optimization attempts.

A second criterion for separating the chosen algorithms is represented by the time required for the evaluation process, respectively the validation process. Thus, in figure 6.18 it is observed that Radius NN has the best training time, of approximately 114 minutes, but the validation time is very long, reaching 2035 min (approximately 34 hours). Interestingly, the

longest training time is the SVC algorithm with RBF kernel, reaching 3575 minutes (approximately 59 hours). This is due to the more complex mathematical model that the SVC algorithm with RBF kernel has.

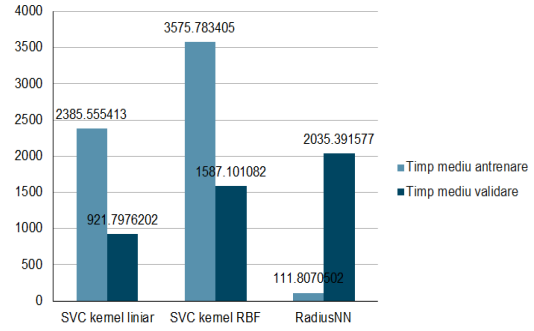

Fig. 6.18. Average training time vs average validation time

Figure 6.19 shows the evolution of the algorithms analyzed during the 3 experiments. Thus, in all cases there is an increase in scores, the most spectacular being in the case of the SVC algorithm with linear kernel, however the best performance, during the 3 experiments, has the SVC algorithm with RBF kernel.

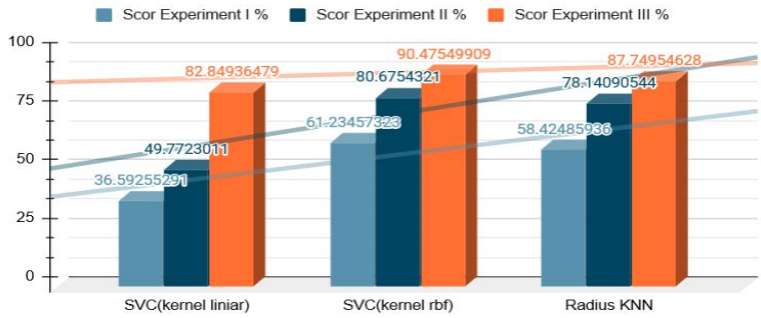

Fig. 6.19. The evolution of thescores of the algorithms analysed during the 3 experiments

Following the optimization, a significant increase can be observed, in relation to the results of experiment II, in the case of the SVC algorithm with linear kernel, the increase reaches up to 14.27%. SVC algorithms with RBF kernel and Radius KNN, also show increases, but not so important.

VI.3.4. Experiment IV – Validation of the chosen algorithms with a newly introduced video frame stream

Normally, in order to check how the Corona discharge is detected in a new data set, the algorithm that performed best in previous experiments should be chosen. A first decision would be to choose the SVC algorithm with RBF kernel, but considering that the results obtained are very similar to those of the Radius NN algorithm and that the SVC algorithm with linear kernel had a spectacular increase after applying the GridSearchCV optimization method. Experiment IV proposes to test all algorithms previously optimized on a data set completely new data set.

The test was performed on the data set acquired by flying over high voltage power lines with an UAV on which an effect similar to the Corona discharge was artificially added. 2 tests were performed, namely on a fraction of 100 images and on a group of 1000 images.

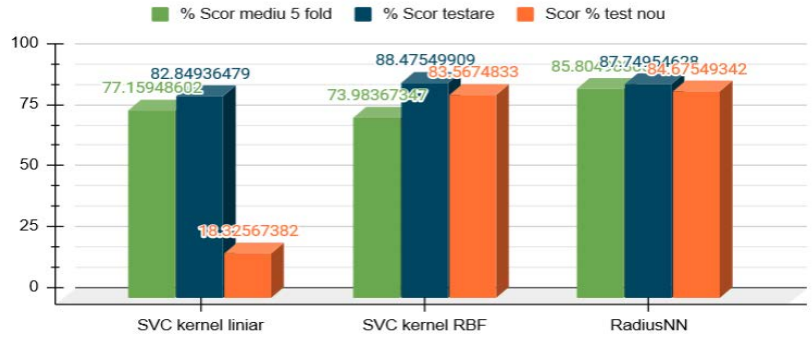

Fig. 6.20. Score of the analysed algorithms with a data set fraction of 100 new video frames

In Figure 6.20, the results obtained can be seen. A first observation is on the spectacular decrease of the results for SVC with linear kernel to only 18.32% accuracy, although after the optimization it had passed the 80% threshold. This observation translates into a major difficulty in adapting the estimator to a data set at first sight despite optimization attempts. Another conclusion is that following the optimization procedure we reached a point of "overfitting"; the model became so specialized in the characteristics of the data set received as input that when a new one was introduced it did not have the ability to predict correctly. We thus demonstrated the hypothesis related to hyper-optimization.

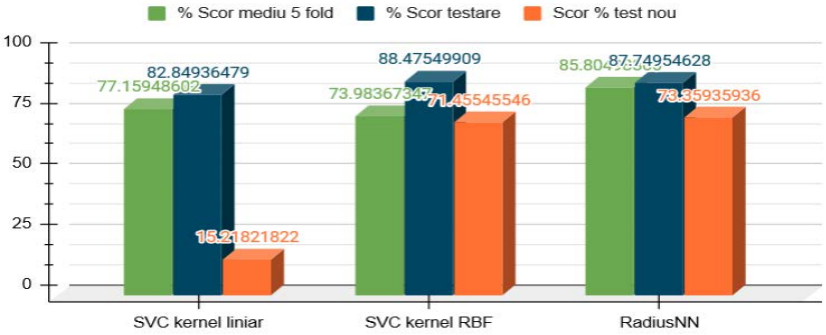

Fig. 6.21. Score of the analysed algorithms with a data set fraction of 1000 new video frames

For the algorithms selected winners in all rounds of experiment, a much better stability and evolution is observed, both in testing with a fraction of 100 new frames and in testing with a data set of 1000 new frames. Although the results are lower than in the last test stage, this was to be expected when working with a completely new data set. However, the decrease is in parameters that still allow their use in a real scenario. The stability of the equation models behind the predictor proposes SVC with RBF and RadiusNN kernel as plausible variants for a real-time classification system of Corona discharge.

Figures 6.22 and 6.23 show the required test times for a data set of 100 frames, respectively for a data set of 1000 frames.

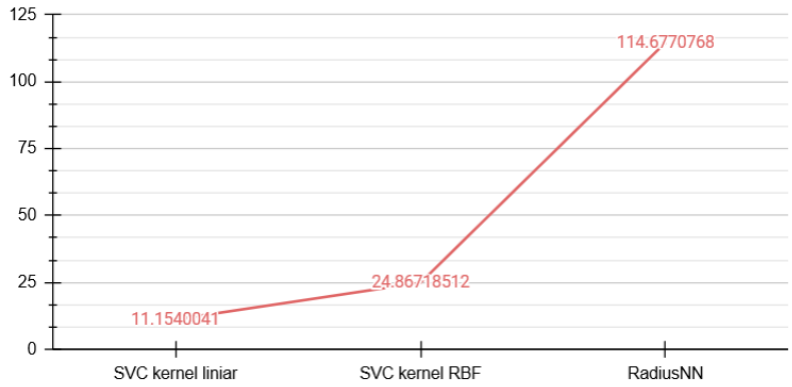

Fig. 6.22. Test time required for 100 video frames

In conclusion, analyzing the results obtained, it is observed that, when introducing a new data set, the score of the analyzed algorithms, except SVC with linear kernel which failed to give a satisfactory result, decreased compared to the score after optimization. These differences are: -7.31% in the case of the SVC algorithm with RBF kernel, respectively -3.07% in the case of the Radius KNN algorithm, having as new data set 100 frames. For the analysis of the new data set of 1000 frames, the results were the following: -19.02% in the case of the SVC algorithm with RBF kernel, respectively -14.39% in the case of the Radius KNN algorithm.

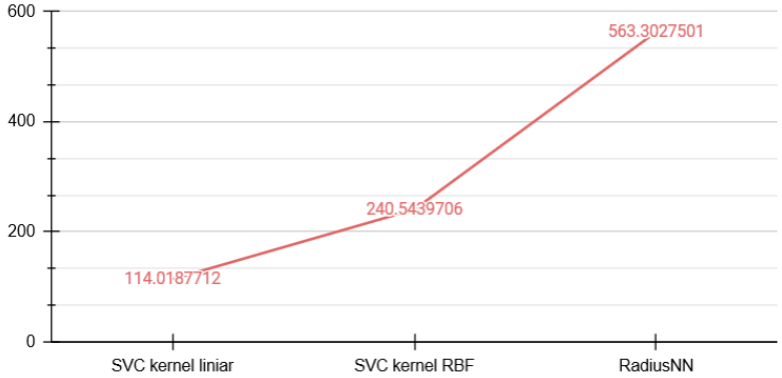

Fig. 6.23. Test time required for 1000 video frames

Table 23: The values ofthe required test times for new data sets

Algorithm		SVC (Linear Kernel)	SVC (RBF Kernel)	Radius KNN
100 frames	Test time required (minutes)	11.15	24.86	114.67
1000 frames	Test time required (minutes)	114.01	240.54	563.30

The final criterion for distinguishing between the two algorithms is given by measuring the required test time. We can see in the graphs displayed that RadiusNN retains its time-consuming character. Although the result of the score is 2% higher than SVC with RBF kernel, the time required for this processing is up to 3 times longer. As this criterion is very important for the project, we propose as a winning estimator the **SVC algorithm with RBF kernel**.

VII. FINAL CONCLUSIONS

This paper presents a series of studies related to the detection of Corona discharge with the help of an unmanned aerial system, in order to reduce the loss of active power on high and very high voltage power lines in Romania.

Chapter I, includes the introduction to the thesis, presenting the approach to the problem from a theoretical and ideological point of view, following an extensive documentation on: the current state of research on the occurrence of Corona discharge on high voltage overhead power lines in Romania, risk factors and causes of occurrence; the current state of use of unmanned aerial vehicle systems to detect Corona discharge, presenting the latest technologies in the field of autonomous climbing robots, hybrids or UAVs capable of performing OHPL inspections.

Chapter II, being entirely dedicated to Corona discharge and its detection methods, concluded that the most effective method for detecting Corona discharge is the use of the UV sensor. Also, with the help of the Matlab-Simulink simulation environment, it was possible to interpolate two Corona loss calculation methods, namely Peek's equation and Peterson's equation, reaching results close to the measurements performed in the real environment, on high voltage power lines.

In Chapter III, a description of the context in which the UAV will be used for flight on the OHPL and an introduction to the field of unmanned aircraft systems where the functional structure of a UAV system was presented.

From a mathematical and graphic point of view, the modeling of a flight is very difficult to achieve, due to its complexity. In Section III.2, an automatic control system has been designed for the control of the flight of the Sky Walker UAV, on the longitudinal channel, in the regime of ascent and maintenance of altitude. Following the calculation of the mathematical model of the longitudinal channel and its simulation in Matlab, using the Simulink module, very good results were obtained in terms of flight altitude control.

Also, a scenario was created following which two sections of a 400 kV overhead power line were compared, one in a mountainous area and the other in a plain area. The comparison resulted in an analysis of the relief, atmospheric conditions and the communication link between the UAV system and the ground station, leading to the conclusion that voltage losses caused by Corona discharge are much more difficult to detect and calculate in the mountainous area.

Chapter IV presents the analysis of the parameters of a test and calibration flight, and the results are presented graphically, revealing a flight stability that gives high confidence for future flight missions on overhead power lines. Also in these graphs it is observed that the real attitude angles of the UAV faithfully follow the commanded attitude angles, thus making the accuracy of the data delivered by the autopilot to be high.

Subchapter IV.1 presents the flight mission on a high voltage line of 400 kV from the OHPL section Brașov - Gutinaș, Brașov county. Following the flight, a number of 5 electirc poles were flown over, and the results of the analysis of the flight parameters were very good.

Thus, the UAV system keeps its flight altitude, relatively constant, the behavior of the attitude angles is good, so that the control on the roll, pitch and yaw angles is closely followed by the UAV.

In conclusion, the designed UAV system responded very well to the calibration tests, the verification flight and, finally, the OHPL overflight mission.

Chapter V proposes an algorithm for detecting, tracking and classifying Corona discharges implemented through a software called CDC (Corona Discharge Classification). This software was entirely my personal contribution, aiming to detect and analyze Corona discharges. After identification, this phenomenon is tracked and processed on board a UAV, specially configured for typical flight missions on high voltage lines.

The Corona landing classification algorithm has been permanently improved with the addition of auxiliary calculation blocks that facilitate the classification process by providing parameters such as: target distance, target coordinates and flight altitude. Also, in the block diagram in fig.5.2, within the Corona discharge detection system, the parameters received from the autopilot and from the RTK system (Real Time Kinematics) are processed, which successfully replaces the GPS system, demonstrating a better accuracy.

The proposal to choose a Corona discharge classification algorithm came based on the analysis of several algorithms specific to supervised learning, as well as unsupervised learning. Their mathematical models were studied in advance and we decided to use only supervised machine learning for the analysis of performance related to score, accuracy and testing time.

In order to demonstrate the choice of the best supervised machine learning algorithm, following the comparison of a number of 8 algorithms, their analysis was carried out during a number of 4 experiments approached in stages.

Therefore, experiment I demonstrates the usefulness of the preprocessing module and highlights the choice of filtering stages leading to an increase in the score as well as the accuracy of the classification algorithms from 10% to 30%.

For experiment number II, to the data set number 1, another data set is added (data set number 2), obtained experimentally in the laboratory and consisting of a number of approximately 1000 video frames representing images recorded by the Corona PCO camera. Ultraviolet on a Corona discharge generating installation. Following experiment II, analyzing the performances of the classification algorithms, it is observed that 2 algorithms stand out, which had consistently good results, namely, SVC with RBF kernel and Radius KNN.

In the case of experiment III for Corona image processing, the optimization of the basic parameters of the analyzed classification algorithms was performed, using the GridSearchCV method, specific to the Python Scikit software package. Following the optimization, a significant increase was observed, compared to the results of experiment II, in the case of the SVC algorithm with linear kernel, an increase of up to 14.27%. SVC algorithms with RBF kernel and Radius KNN also show increases, but not so important.

Experiment IV was dedicated to the validation of the chosen algorithms with a newly introduced data set. Thus, the test was performed on the data set purchased by flying over the airspace with a UAV device on which an effect similar to the Corona discharge was artificially added. In experiment IV, 2 tests were performed, namely on a fraction of 100 images and on a group of 1000 images.

For the algorithms selected winners in all rounds of experiment, a much better stability and evolution was observed comparatively, both in testing with a fraction of 100 new frames and in testing with a data set of 1000 new frames. Although the results are lower than in the last test stage, this was to be expected when working with a completely new data set. However, the decrease is in parameters that still allow their use in a real scenario. The stability of the equation models behind the predictor proposes SVC with RBF and RadiusNN kernel as plausible variants for a real-time classification system of Corona discharge. However, the final criterion for distinguishing between the two algorithms was given by measuring the required test time. Thus, comparing the performances related to the necessary testing time of the 2 algorithms, it is observed that RadiusNN keeps its time-consuming character. Although the result of the score is 2% higher than SVC with RBF kernel, the time required for this processing is up to 3 times longer. As this criterion is very important for the project, the winning estimator and my proposal for the realization of a Corona discharge classification system, is the SVC algorithm with RBF kernel.

Based on the above, I consider that the doctoral thesis entitled "Contributions to the development of a system for monitoring losses on high voltage power lines by surveillance with unmanned aircraft" has achieved its purpose for which it was proposed by bringing elements of novelty both in the field of unmanned aerial vehicle systems flying on high voltage lines and in the processing of the video signal received from the Corona camera in order to detect, track and classify the Corona discharge.

VIII. PERSONAL CONTRIBUTIONS AND FUTURE DIRECTIONS

Based on the above, it can be argued that the doctoral paper presented contains significant personal contributions, both conceptually, by the proposal to fly over high voltage power lines with a system of unmanned aircraft with fixed wing at the expense of UAVs with rotating wing, as well as on a practical level by executing specific flights with the UAV system specially designed and configured for flights in order to detect, track and classify the Corona discharge.

In order to demonstrate the negative effects of Corona discharge and to highlight the magnitude of losses on the OHPL, a numerical simulation model was developed, using the Matlab - Simulink program, which is based on the analytical formulas for calculating Corona losses, namely its Peek‟s formula and Peterson's formula.

Also, the design of a flight path specific to high voltage power lines based on an analysis of the landforms, the atmospheric factor and the data link of the UAV with the ground control station, is a personal contribution.

Performing the numerical simulation of an automatic control system for the control of the flight of the Skywalker UAV, on the longitudinal channel, in regime of ascent and maintenance of altitude is considered a personal contribution.

The verification and calibration flights of the UAV parameters, performed on Sânpetru aerodrome, as well as the actual flights on the 400 kV high voltage line, Brașov - Gutinaș, were

successfully performed, and after them the UAV parameters were analysed, so that it was able to maintain the scheduled flight route and maintain a stable altitude throughout the mission.

Conceptually developing and proposing an idea to approach Corona discharge classification by creating CDC (Corona Discharge Classification) software is, in my view, the greatest personal achievement of this paper. Also, the demonstration of the functionality, from a mathematical point of view, of the target tracking blocks (Corona discharge), of the target distance calculation block and of the target coordinate calculation block represents a great achievement in the context of implementing these calculations on board UAVs, executed in real time.

All 4 data sets used in the analysis of supervised machine learning algorithms are own contribution and were acquired by original and own methods.

The presentation of some of the results of the scientific effort, which was the basis for the elaboration of the doctoral thesis, in national and international scientific conferences, confirms the originality and novelty of the results obtained.

Among the future research directions, we can mention the processing of video images from the Corona camera with the implementation of better artificial intelligence algorithms (neural networks, deep learning) that can increase the accuracy and score of the Corona discharge, as well as estimating possible losses, based on extracting white pixels from the analyzed video frames.

The development of a user-commandable results display application, as well as the physical and software implementation of all mathematically designed and demonstrated blocks on board a UAV system, is a future priority.

As future work, I propose to find an equation that connects the two dynamic systems of the project: the unmanned aerial vehicle system and the Corona discharge phenomenon, using as variable parameters: UAV flight speed, target distance, flight altitude and flight speed. pixel shift in a region of interest (ROI), automatically defined when the Corona discharge occurs in video frames.

Another thing I propose in the near future is to create a new set of flights that will become more conclusive than the previous ones and that will strictly follow the flight route created especially for flights on the OHPL.

Implementing the algorithm performed on the Nvidia TX2 processing board and evaluating the computation times so that the algorithm as a whole is reliable for the analysis of a large number of video frames, is also a future priority.

Given the above, the project opens new directions of research and can be analyzed for implementation at the industrial level in electricity transmission companies.

Selective Bibliography

1. Transelectrica –"Strategia energetică a României pentru perioada 2007 - 2020 actualizată pentru perioada 2011 – 2020".
6. G. Dong, X. Chen, B. Wang, J. Zhang, L. Liu, Q. Wang, and C. Wei, "Inspecting transmission lines with an unmanned fixed-wings aircraft," in Applied Robotics for the Power Industry (CARPI), 2012 2nd International Conference on, Sept 2012, pp. 173–174.
7. H. Sharma, R. Bhujade, V. Adithya, and P. Balamuralidhar, "Visionbased detection of power distribution lines in complex remote surroundings," in Communications (NCC), 2014 Twentieth National Conference on, Feb 2014, pp. 1–6.
8. Z. Li, T. S. Bruggemann, J. J. Ford, L. Mejias, and Y. Liu, "Toward automated power line corridor monitoring using advanced aircraft control and multisource feature fusion," Journal of Field Robotics, vol. 29, no. 1, pp. 4–24, 2012.
20. Luis F. Luque-Vega, Bernardino Castillo-Toledo, Alexander Loukianov, Luis Enrique Gonzalez-Jimenez, Power Line Inspection Via an Unmanned Aerial System Based on the Quadrotor Helicopter, 17th IEEE Mediterranean Electrotechnical Conference, Beirut, Lebanon, 13-16 April 2014.
21. https://www.thedroneu.com/blog/how-to-use-drones-for-powerline-inspections/
22. M. Nayyerloo, X. Chen, W. Wang, JG Chase, "Cable-Climbing Robots for Power Transmission Lines Inspection", Mechanical Engineering Department, University of Caterbury, Chrischurch, New Zealand.
24. W. Chang, G. Yang, J. Yu, Z. Liang, L. Chen, C. Zhou, "Development of a Power Line Inspection Robot with Hybrid Operation Modes", International Conference on Intelligent Robots and Systems (IROS), IEEE, ISSN**:** 2153-0866, 24-28 September, 2017.
26. Joseph L. Moore, "Powerline Perching with a Fixed-Wing UAV", Department of Mechanical Engineering, Massachusetts Institute of Technology, June, 2011.
27. Maxim Lu, Alex James, Mahdi Bagheri, "Unmanned Aerial Vehicle (UAV) charging from powerlines", IEEE PES Asia-Pacific Power and Energy Engineering Conference (APPEEC), Bangalore, India, 8-10 November, 2017.
28. Milan Simic, Cees Bil, Vuk Vojisavljevic, "Investigation in Wireless Power Transmission for UAV Charging", Procedia Computer Science, Volume 60, 2015, pp. 1846-1855.
29. L. Matikainena, M. Lehtomakia, E. Ahokasa, J. Hyypp ¨ aa, M. Kar- ¨ jalainena, A. Jaakkolaa, A. Kukkoa, and T. Heinonenb, "Remote sensing methods for power line corridor surveys," ISPRS Journal of Photogrammetry & Remote Sensing, vol. 119, pp. 10-31., 2016.
30. D. I Jones and G. K Earp, "Camera sightline pointing requirements for aerial inspection of overhead power lines," Electric Power Systems Research, vol. 57, no. 2, pp. 73-82, 2001.
32. Andrew J. Moore, Matthew Schubert, Nicholas Rymer, "Autonomous Inspection of Electrical Transmission Structures with Airborne UV Sensors NASA Report on Dominion Virginia Power Flights of November 2016", NASA/TM–2017-219611, Langley Research Center, https://www.flir.com/suas/uas-for-utility-inspection/
33. Yin Limin, Zhangyu L., "Ultraviolet Image Processing Method in Corona Discharge", Second International Workshop on Computer Science and Engineering, 2009.
43. Y. Kim and K. Shong, "The Characteristics of UV Strength According to Corona Discharge from Polymer Insulators Using a UV Sensor and Optic Lens", IEEE Transactions on Power Delivery, Vol. 26, No. 3, 2011, pp. 1579-1585.
44. W.T. Hu and S. H. Wang, "Brief Discussion on Influence Factors in Detecting Corona Discharge by UV Detector", North China Electric Power, No. 1, 2009.
45. L. Chen, X. M. Bian, F. L. Chen, X. B. Meng, L. M Wang and Z. C. Guan, "Method to Judge Corona Incep-tion Voltage of AC Transmission Lines Using Corona Cage", High Voltage Engineering, Vol. 37, No. 1, 2011, pp. 85-90.
70. Popovici D., Lolea M.,"Tehnica tensiunilor înalte", Facultatea de Energetică, Universitatea din Oradea, 2011.
76. Evan Mayerhoff,"Corona and its effects", High Voltage Connection, Inc., 2007.

96. Enesi Asizehi Yahaya, Tsado Jacob, Mark Nwohu, Ahmed Abubakar, "Power loss due to Corona on High Voltage Transmission Lines", IOSR Journal of Electrical and Electronics Engineering (IOSR-JEEE), Volume 8, Issue 3 (Nov. - Dec. 2013), PP 14-19.
97. Drăgan Gleb – Tehnica tensiunilor înalte, Volumul I, Ed. Tehnică, Bucureşti, 1996.
98. J. B. Gupta, "A course in power systems", S. K. Kataria & Sons, New Delhi, 2008.
99. C. L. Wadwah "Electric Power System" Chennai, New Age International. Publisher Ltd, 2006.
100. B. R. Gupta "Power system analysis and design" S. Chand, New Delhi, 2007.
102. Samuel C. Hassler and Fulya Baysal-Gurel," Unmanned Aircraft System (UAS) Technology and Applications in Agriculture", Agronomy Journal, 9 October 2019.
146. Juraj Micek, Jan Kapitulik, "Median Filter", Journal of Information, Control and Management Systems, Vol.1, (2003), No.2.
148. Prakhar Ganesh,"Types of Convolution Kernels: Simplified", Towards Data Science, Computer Vision and Deep Learning Section, October, 2019.
156. Hsin-Yuan Huang, Chih-Jen Lin, "Linear and Kernel Classification: When to use Which?", Department of Computer Science, National Taiwan University.
159. H.-F. Yu, F.-L. Huang, and C.-J. Lin. Dual coordinate descent methods for logistic regression and maximum entropy models. MLJ, 85:41–75, 2011.
160. V. Vapnik. Statistical Learning Theory. Wiley, New York, NY, 1998.
162. https://scikit-learn.org/stable/modules/cross_validation.html

List of scientific papers

1. **Vidan Cristian**, Jula Nicolae, Martin Timmerman, Robby Haelterman, "*Detection Of High Voltage Lines Based On Analyzing Images Received From An Uav In Order To Detect Corona Discharge"*, KBO Conference, 11-13 June 2015, Sibiu, Romania, WOS:000379493200128, ISSN: 1843-6722

2. Răzvan-Viorel Mihai, **Cristian Vidan**, Radu-Călin Pahonie, Pericle Matei, Adrian Mihail Stoica, Ioana Adochiei, "*A Semi-Autonomous Small Scale Paramotor Used for Medical Emergency Situations*", The 5th Edition of the International Conference on e-Health and Bioengineering (EHB 2015), 19-21 November 2015, Iasi, Romania, WOS:000380397900184, ISBN:978-1-4673-7545-0, ISSN: 2575-5137.

3. Ioana Edu (Adochiei), Teodor Lucian Grigorie, Felix Adochiei, Petre Negrea, **Vidan Cristian**, Nicolae Jula, "*Assistive Inertial 3D Positioning MEMS System*", The 5th Edition of the International Conference on e-Health and Bioengineering (EHB 2015), 19-21 November 2015, Iasi, Romania, WOS:000380397900189, ISBN:978-1-4673-7545-0, ISSN: 2575-5137.

4. **Vidan Cristian** " *Lateral Guidance Laws For Autonomous Tracking Flight Paths",* The 18 edition of International Conference „Scientific Research and Education in the Air Force-AFASES 2016", 26-28 May 2016, Brasov, Romania.

5. **Vidan Cristian**, Badea Silviu-Ionut, "*Longitudinal automatic control system for a light weight aircraft"*, International Conference of Aerospace Sciences (AEROSPATIAL 2016), 26-27 october 2016, Bucharest, Romania.

6. **Vidan Cristian**, Mărăcine Mihaela, "*Corona discharge classification based on UAV data acquisition*", The 21th International Conference on Control Systems and Computer Science (CSCS21), 29-31 may 2017, Bucharest, Romania, WOS:000449004400099, ISBN:978-1-5386-1839-4

7. **Vidan Cristian**, Maracine Daniel "*Studying the possibility of increasing the flight autonomy of a rotary wing MUAV",* The 19 edition of International Conference „Scientific Research and Education in the Air Force-AFASES 2017", 26-28 May 2017, Brasov, Romania.

8. **Vidan Cristian,** Alexandru Gavril, Mihai Razvan, Catargiu Florin, *"On-board UAV video processing for ground target tracking",* The 20th edition of International Conference „Scientific Research and Education in the Air Force-AFASES 2018", 22-27 May 2018, Brasov, Romania.

9. Florin CATARGIU, **Cristian VIDAN**, Răzvan MIHAI, Gavril ALEXANDRU,*"Helical Antenna Design for Automated UAV Tracking System",* MTA Review Magazine, XXVIII, Military Technical Academy, Bucharest, 2018.

10. Marian Gaiceanu, Silviu Epure, Cristinel Radu Dache, Razvan Buhosu, Iulian Ghenea, **Cristian Vidan**, *"Laboratory power inverter platform for variable speed drive",* 5th International Symposium on Electrical and Electronics Engineering (ISEEE), 20-22 Oct. 2017, Galați, Romania, WOS:000428234400065, ISBN:978-1-5386-2059-5, ISSN: 2378-3907.

11. Marian Gaiceanu, Razvan Buhosu, Iulian Ghenea, **Cristian Vidan**,*"Complete regenerative distributed drive system",* 5th International Symposium on Electrical and Electronics Engineering (ISEEE), 20-22 Oct. 2017, Galați, Romania, WOS:000428234400063, ISBN:978-1-5386-2059-5, ISSN: 2378-3907.

12. **Cristian Vidan**, Răzvan-Viorel Mihai, Marian Găiceanu, George Alexandru Ilie, "*Designing and altitude controller* for a *miniUAV using an automated speed device*", ICNPAA 2018, Mathematical, Problems in Engineering, Aerospace and Science, 16-17 July 2018, Yerevan, Armenia, WOS:000468353100104, ISBN:978-0-7354-1772-4, ISSN: 0094-243X.

13. Mihai Razvan-Viorel, **Vidan Cristian**, Gavril Alexandru, Alexandru Radu, *"Cooperative distrubuted collision avoidance estimates in a dynamic environment for a heterogenous UAV formation",* ICNAAM 2018, 16th International Conference of Numerical Analysis and Applied Mathematics, 13-18 September 2018, Rhodes, Greece, AIP Conference Proceedings 2116, 360007 (2019); https://doi.org/10.1063/1.5114367.

14. **Vidan Cristian**, Mihai Razvan-Viorel, Sava Cristina, Gaiceanu Marian, Tăban Ovidiu, Catargiu Florin, *"UAV Mission Planning Interface development with trajectory optimization algorithm",* ICNAAM 2018, 16th International Conference of Numerical Analysis and Applied Mathematics, 13-18 September 2018, Rhodes, Greece, AIP Conference Proceedings 2116, 360006 (2019); https://doi.org/10.1063/1.5114366.

Research projects

1. Advanced system for reducing losses in the transport of utilities of strategic interest, based on IT infrastructure and autonomous air surveillance (INSAV). Sectoral Operational Program Increasing Economic Competitiveness, Priority Axis 2 - Competitiveness through RDI, Operation 2.3.3: Promoting innovation in enterprises. Nr. Project: 1752 / SMIS Code - CSNR 47532. Duration: 2013-2016 (33 months) - Member of the research team. Link: http://www.insoft-dc.ro/insav

2. UAV platforms (unmanned aerial vehicles) with dedicated capabilities and support infrastructure, for applications in national security missions (UAVino). Sectoral Operational Program Increasing Economic Competitiveness, Prior Axis. 2 - Compet. through CDI. Duration: 36 months - Member of the research team.Link: http://www.incas.ro/images/stories/PN-III/UAVino/index.html - **PN-III-P2-2.1-SOL-2016-01-0008.**

3. Solutions and systems for monitoring and aerial work activities in support of the public health system in case of the COVID-19 pandemic using UAS systems, Program from PN III: Increasing the competitiveness of the Romanian economy through research, development and innovation - Member of the research team. **PN-III P2-2.1-SOL-2020-2-0329**.

4. Development of ventilator prototypes with parameters adapted to assist patients infected with the SARS-CoV-2 virus. Program from PN III: Increasing the competitiveness of the Romanian economy through research, development and innovation - Member of the research team. PN-III P2-2.1-SOL-2020-2-0337**.**

5. Experimental platform for testing and evaluating equipment and systems compatible with the MIL-STD-1553 communications standard. Sectoral research and development plan of the Ministry of National Defense for 2019. Plan position: 90 - project coordinator.

6. Unmanned aerial system for surveillance and research with the possibility of performing kinetic actions. Sectoral research and development plan of the Ministry of National Defense for 2019. Plan position: 168 - **project coordinator**.

7. Use of autonomous submersible vehicles in mine action. Sectoral research and development plan of the Ministry of National Defense for 2019. Plan position: 145 - **project coordinator**.